Title

SUMO fosters assembly and functionality of the MutSγ complex to facilitate meiotic crossing over

Journal

Developmental Cell, 56(14)

ISSN

1534-5807

Authors

He, Wei
Verhees, Gerrik F
Bhagwat, Nikhil
et al.

Publication Date

2021-07-01

DOI

10.1016/j.devcel.2021.06.012

Peer reviewed

HHS Public Access

Author manuscript

Dev Cell. Author manuscript; available in PMC 2022 July 26.

Published in final edited form as:

Dev Cell. 2021 July 26; 56(14): 2073–2088.e3. doi:10.1016/j.devcel.2021.06.012.

SUMO Fosters Assembly and Functionality of the MutSγ Complex to Facilitate Meiotic Crossing Over

Wei He[1,2], **Gerrik F. Verhees**[2,†], **Nikhil Bhagwat**[1,2], **Ye Yang**[1,2], **Dhananjaya S. Kulkarni**[1,2], **Zane Lombardo**[3], **Sudipta Lahiri**[3,‡], **Pritha Roy**[2], **Jiaming Zhuo**[2], **Brian Dang**[2], **Andriana Snyder**[2], **Shashank Shastry**[2], **Michael Moezpoor**[2], **Lilly Alocozy**[2], **Kathy Gyehyun Lee**[2], **Daniel Painter**[2], **Ishita Mukerji**[3], **Neil Hunter**[1,2,*]

[1]Howard Hughes Medical Institute, University of California, Davis, Davis, California, USA.

[2]Department of Microbiology & Molecular Genetics, University of California, Davis, Davis, California, USA.

[3]Department of Molecular Biology and Biochemistry, Molecular Biophysics Program, Wesleyan University, Middletown, Connecticut, USA.

SUMMARY

Crossing over is essential for chromosome segregation during meiosis. Protein modification by SUMO is implicated in crossover control but pertinent targets have remained elusive. Here we identify Msh4 as a target of SUMO-mediated crossover regulation. Msh4 and Msh5 constitute the MutSγ complex that stabilizes joint-molecule (JM) recombination intermediates and facilitates their resolution into crossovers. Msh4 SUMOylation enhances these processes to ensure that each chromosome pair acquires at least one crossover. Msh4 is directly targeted by E2 conjugase Ubc9, initially becoming mono-SUMOylated in response to DNA double-strand breaks, then multi/poly-SUMOylated forms arise as homologs fully engage. Mechanistically, SUMOylation fosters interaction between Msh4 and Msh5. We infer that initial SUMOylation of Msh4 enhances assembly of MutSγ in anticipation of JM formation, while secondary SUMOylation may promote downstream functions. Regulation of Msh4 by SUMO is distinct and independent of its previously described stabilization by phosphorylation, defining MutSγ as a hub for crossover control.

eTOC Blurb

*Correspondence to lead contact: Neil Hunter, nhunter@ucdavis.edu.
†Current address: Institute of Physiological Chemistry, Medical Faculty Carl Gustav Carus, Technische Universitaet Dresden, Dresden, Germany.
‡Current address: Department of Therapeutic Radiology, Yale University School of Medicine, New Haven, Connecticut, USA

AUTHOR CONTRIBUTIONS

W.H. and N.H. conceived the study and designed the experiments. Y.Y. and N.B performed *in vitro* SUMOylation experiments and proteomics analysis. W.H., G.V., P.R., J.Z., B.D., A.S., and S.S. performed yeast tetrad analysis. W.H., G.V., P.R., J.Z., B.D., M.M. and L.A. prepared and analyzed chromosome spreads. Z.L, S.L. and I.M. performed molecular modeling of MutSγ. W.H. and N.H. wrote the manuscript with inputs and edits from all authors.

DECLARATION OF INTERESTS

The authors declare no competing interests.

Meiotic crossovers promote accurate chromosome segregation. He et al. show that SUMO modifies the recombination factor Msh4, enhancing its interaction with Msh5 to assemble the MutSγ complex, which promotes crossovers. Msh4 SUMOylation requires DNA double-strand breaks, defining a pathway that couples the initiation of recombination to crossover control.

Graphical Abstract

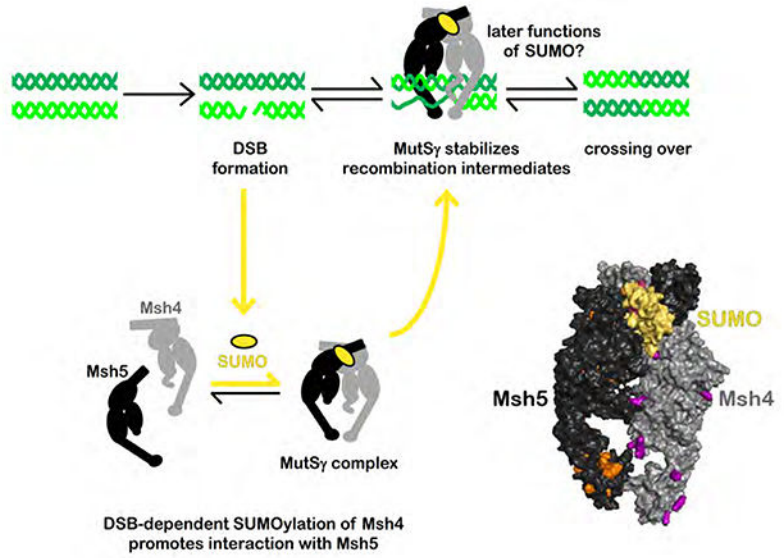

INTRODUCTION

During sexual reproduction, haploid gametes are produced via the two successive rounds of chromosome segregation that occur in meiosis. Accurate segregation at the first meiotic division (MI) requires homologous chromosomes to pair and become connected by crossovers that enable stable biorientation on the MI spindle (Hunter, 2015; Watanabe, 2012). Crossover number and distribution are controlled to ensure that each homolog pair obtains at least one crossover (assurance) and that adjacent crossovers are widely and evenly spaced (interference)(Saito and Colaiacovo, 2017; Wang et al., 2019). Defects in crossover distribution leads to errors in meiosis that contribute to infertility, miscarriage and some congenital diseases (Herbert et al., 2015; Hunter, 2015; Kim et al., 2016; Wang et al., 2017).

The mechanisms underlying crossover control are not well understood, but protein modification by SUMO (Small Ubiquitin-like MOdifier) has been implicated by several studies (Bhagwat et al., 2021; Cheng et al., 2006; Hooker and Roeder, 2006; Leung et al., 2015; Lin et al., 2010; Qiao et al., 2014; Rao et al., 2017; Reynolds et al., 2013; Serrentino et al., 2013; Voelkel-Meiman et al., 2019; Voelkel-Meiman et al., 2013; Zhang et al., 2014). The 11 KDa SUMO protein is a dynamic reversible modification of lysine (K) sidechains catalyzed by a cascade of enzymes that activate (E1) snd conjugate (E2) SUMO; and confer

target specificity (E3 ligases)(Gareau and Lima, 2010). SUMO is deconjugated by a family of dedicated cysteine proteases (Nayak and Muller, 2014). Protein SUMOylation regulates many basic cellular pathways, including various aspects of chromosome metabolism and cell cycle regulation (Dhingra and Zhao, 2019; Gareau and Lima, 2010; Jentsch and Psakhye, 2013; Kerscher et al., 2006; Zhao, 2018). At the level of individual target proteins, SUMOylation can alter activity in a number of ways including steric hinderance, conformational change, stabilization, competition with other lysine modifications (ubiquitination and acetylation), degradation via SUMO-targeted ubiquitin ligases and mediating protein-protein interactions through SUMO-interaction motifs (Almedawar et al., 2012; Flotho and Melchior, 2013; Liebelt and Vertegaal, 2016; Papouli et al., 2005; Steinacher and Schar, 2005; Zhao, 2018).

The DNA steps of meiotic recombination are coupled to the dramatic chromosome dynamics that occur during meiotic prophase I (Hunter, 2015). Programmed double-strand breaks (DSBs) occursonsreplicated chromosomes and outnumber crossovers by ~2–30 fold, depending on the species. DSB ends are resected to produce long-single stranded tails (~800 nt)(Mimitou et al., 2017; Zakharyevich et al., 2010) that assemble into nucleoprotein filaments, comprising RecA-family proteins Dmc1 and Rad51, and catalyze homolog search and strand exchange to form nascent joint-molecule (JM) intermediates called D-loops (Brown and Bishop, 2014). These pairing interactions help bring homologs into close proximity and enable their synapsis, which involves installation of the synaptonemal complex central region along the lengths of coaligned homolog axes (Zickler and Kleckner, 2015). Crossover and non-crossover pathways appear to differentiate at this juncture with non-crossover products arising primarily via synthesis-dependent strand annealing, in which D-loops are extended by DNA synthesis before the invading strand is displaced and annealed to the other DSB end. Crossover recombination proceeds via a metastable JM called the Single-End Invasion (SEI) intermediate which matures in the context of fully synapsed chromosomes into a double-Holliday Junction (dHJ)(Hunter and Kleckner, 2001; Lao et al., 2008; Schwacha and Kleckner, 1995). Biased dHJ resolution produces crossover products before homologs desynapse and prepare for segregation at the first meiotic division (Allers and Lichtes, 2001; Cannavo et al., 2020; Kulkarni et al., 2020; Zakharyevich et al., 2012)s

Modulation of each step of meiotic recombination can impinge on crossover control including the number, locations and timing of programmed DSBs; recombination template choice (homolog versus sister chromatid); and the maturation and resolution of JMs. It is becoming clear that SUMOylation influences each of these steps. Notably, our recent execution-point analysis of SUMO function in budding yeast, using degron alleles of the E1 enzyme Aos1- Uba2, revealed roles in DSB formation, JM metabolism, synapsis, crossing over and meiotic progression (Bhagwat et al., 2021). Similarly, in mammals, chemical inhibition of SUMOylation in short-term cultures of mouse spermatocytes caused defects in synapsis, recombination and the progression of meiotic prophase I (Rao et al., 2017). Moreover, meiosis-specific SUMO E3- ligases related to budding yeast Zip3 and mammalian RNF212 specifically accumulate at prospective crossover sites and are required for crossing over at these locations (Henderson and Keeney, 2004; Qiao et al., 2014; Rao et al., 2017; Reynolds et al., 2013; Serrentino et al., 2013; Zhang et al., 2014). However, the

identity of pertinent targets and our understanding of how SUMO regulates their activity to promote crossing over remain major challenges.

Zip3/RNF212 are members of an unrelated group of pro-crossover factors originally defined in budding yeast called the ZMMs (Zip1–4, Mer3, Msh4 and Msh5)(Hunter, 2015). These include the major component of synaptonemal complexes (Zip1) and three enzymes that directly interact with recombination intermediates: the Zip2-Spo16 complex related to XPF-ERCC1 endonucleases (Arora and Corbett, 2019; De Muyt et al., 2018; Guiraldelli et al., 2018; Macaisne et al., 2011; Zhang et al., 2019), DNA helicase Mer3 (Chen et al., 2005; Duroc et al., 2017; Guiraldelli et al., 2013; Mazina et al., 2004; Nakagawa and Kolodner, 2002) and the MutSγ complex comprising Msh4 and Msh5, two homologs of the mismatch repair factor MutS (Manhart and Alani, 2016; Snowden et al., 2004). Our analysis of SUMO function during meiosis in mouse points to the ZMMs as candidate targets (Qiao et al., 2014; Rao et al., 2017; Reynolds et al., 2013); and using global proteomics approaches in budding yeast we recently revealed that all the ZMMs, with the exception of Spo16, are indeed SUMOylated (Bhagwat et al., 2021). Here, we show that regulation of MutSγ by SUMO is important for crossover control.

RESULTS

Mapping of SUMOylation Sites on Msh4

To test the idea that MutSγ might be a target of meiotic SUMOylation, Msh4 and Msh5 were separately immunoprecipitated (IP) from budding yeast cultures undergoing synchronous meiosis and analyzed by Western blot using an antibody against Smt3 (hereafter SUMO; Figures 1A and S1). Msh4 SUMOylation was detected at the 4 and 6 hr timepoints, as JMs form and chromosome synapsis ensues. A ladder of three SUMOylated forms was apparent in Msh4 IP Westerns (indicated by white dots in Figure 1A). The most prominent form appeared earlier and migrated just above the position of phosphorylated Msh4 (indicated by a green asterisk in Figure 1A), at a position consistent with mono-SUMOylation. Slower migrating forms could be the result of co-modification by SUMO and phosphorylation, or multi- or poly- SUMOylation of Msh4 (i.e. respectively, Msh4 conjugated to a single SUMO moiety at two or more sites; or conjugated to a polymeric SUMO chain at a single site; see below). Unlike Msh4, SUMOylation of Msh5 was not detectable by IP Western (Figure S1A).

Two approaches were taken to map the SUMO conjugation sites on Msh4 (Figures 1B–D and S2). *In vitro* SUMOylation of purified MutSγ showed that Msh4 but not Msh5 could be modified (Figure 1B and S2), consistent with our IP Western data. *In vitro* SUMOylation did not require an E3 ligase indicating that Msh4 can be directly modified by the E2 conjugase Ubc9. However, conjugation efficiency was enhanced in the presence of the meiosis-specific E3 ligase, Zip3, likely because of its ability to generally stimulate Ubc9 activity (Cheng et al., 2006). A scaled up *in vitro* SUMOylation reaction and SDS-PAGE were used to isolate modified forms of Msh4, which were then digested with trypsin and subject to LC-MS/MS (Figure 1C and S2). Four conjugation sites were mapped using this approach: lysines 29, 33, 34 and 205. Given that the native branched SUMO remnant produced by trypsin digestion (K-ε-GGIQE) is inefficiently detected by standard LC-MS/MS approaches (Wohlschlegel et

al., 2006), and sites mapped from *in vitro* SUMOylation might not accurately reflect those modified *in vivo,* we pursued a second approach to map SUMOylation sites on Msh4 as part of our large-scale effort to delineate the SUMO-modified meiotic proteome *in vivo* (Bhagwat et al., 2021). This approach employed a hexa-histidine tagged native *SMT3* gene carrying an I96K mutation, which yields a K- ε -GG di-glycine SUMO conjugation remnant upon digestion with LysC (Figure 1D)(Wohlschlegel et al., 2006). This construct enabled a tandem affinity approach to first enrich for SUMO conjugates under denaturing conditions, using immobilized metal-affinity chromatography, and then affinity purify di-glycine branched SUMO-peptides which were subject to LC-MS/MS (Wohlschlegel et al., 2006; Xu et al., 2010). Using this approach an additional eight SUMOylated lysines were mapped on Msh4 at residues 53, 177, 476, 478, 530, 784, 819 and 834 (Figure 1E). Although SUMOylation of Msh5 was not detected by IP Western (Supplemental Figure S1A) and Msh5 was not modified *in vitro* (Figure 1B), our global proteomics approach identified three modified sites on Msh5 (Supplemental Figure S1B)(Bhagwat et al., 2021). However, these sites appeared to be inconsequential for Msh5 function (Supplemental Figure S1D,E).

The 12 identified Msh4 SUMOylation sites were scattered throughout the polypeptide, with the exception of MutS domain III (Figure 1E and Supplemental Figure S3A). Mapping of these SUMOylated lysines on a structure-based homology model of *S. cerevisiae* MutSγ (Figure 1F and Supplemental Figure S3B)(Lahiri, 2019) suggests that all sites are surface exposed, and thus accessible to the SUMO machinery, and the majority (9/12, or 11/14 considering that K53 is part of a lysine triplet 51-KKK-53) are located on a single face of Msh4. Two sites, K819 and K834 lie in the C-terminal dimerization domain at a potential interface between Msh4 and Msh5. K177 also lies close to an interface between Msh4 and Msh5. Lysines 29, 33, 34 and 530 lie in the lower cavity regions likely to interact with DNA, suggesting that SUMOylation at these sites could alter joint-molecule binding by MutSγ. 51-KKK-53 are located on the inside surface of the upper cavity between Msh4 and Msh5, and SUMOylation at this location may also perturb DNA binding. Finally, K784 is located in the Msh4 ATPase domain.

To confirm that identified sites account for all Msh4 SUMOylation detected *in vivo,* target lysines were mutated to arginine and the K-to-R derivative was subjected to IP-Western analysis (Figures 1F,G). For this analysis, the two additional lysines, K51 and K52, that are potentially redundant with the mapped K53 conjugation site, were also mutated. The 14 site msh4–14KR protein was not SUMOylated indicating that all conjugation sites had been identified (Figure 1G; note that twice the amount of immunoprecipitated material was loaded for msh4–14KR samples to rule out the possibility that Msh4 was still being SUMOylated at a very low-level). The conservative K-R changes in msh4–14KR are not predicted to perturb the MutSγ structure (Supplemental Figure S3C).

SUMOylation Of Msh4 Is Required For Efficient Crossing Over And Crossover Control

The role of Msh4 SUMOylation in crossing over was assessed by measuring genetic map distances in wild-type, *msh4–14KR* and *msh4*Δ strains in a background carrying markers on three different chromosomes (III, VII, and VIII; Figure 2A). Cumulative map distances for each chromosome showed that the *msh4*Δ null mutation reduced crossing over by 2.1 to 2.8-

fold relative to wild type (Figure 2B, Supplemental Figure S4 and Tables S2). Overall, 55% of all crossovers were Msh4 dependent. Crossover reductions of 1.4 to 1.6-fold were seen for the SUMOylation-defective *msh4–14KR* allele from which we infer that SUMOylation is required for 58% of Msh4-dependent crossovers, i.e. the crossover function of Msh4 is partially dependent on its SUMOylation. We also assessed whether the subsets of SUMOylation sites mapped *in vitro* or *in vivo* (Figure 2B–D) made different contributions to the crossover function of Msh4 (Supplemental Figure S5 and Table S4). This analysis suggests that SUMOylation at the N-terminal sites mapped *in vitro* (K29, K33, K34 and K205) is more important than modification at the other mapped sites.

ZMM mutants show elevated levels of gene conversions because DSBs continue to form when homolog engagement is defective (Thacker et al., 2014). Accordingly, the *msh4*Δ null mutant showed a 3.4-fold increase in cumulative gene conversion frequency for the 12 markers in this background (Figure 2C, Supplemental Figure S4 and Supplemental Table S3). By contrast, gene conversions were increased by 2.1-fold in *msh4–14KR* cells, consistent with a partial defect in Msh4 function in the absence of SUMOylation.

The ≤1.6-fold reduction in crossover rate seen in *msh4–14KR* cells would reduce the global crossover numbers from an average of ~90 per cell to ~56, which is theoretically more than enough to ensure ≥1 crossover for each the 16 chromosome pairs of budding yeast. Thus, non-exchange chromosomes and nondisjunction are not an inevitable consequence of reduced crossing over in *msh4–14KR* cells unless crossover control is also defective. To determine whether the efficiency of crossover assurance is enhanced by Msh4 SUMOylation we employed a strain carrying eight linked intervals spanning the entire length of chromosome III (Figure 2D and Supplemental Table S2)(Lao et al., 2013b; Zakharyevich et al., 2010). In wild-type, just 1.3% of tetrads lacked a detectable crossover between chromosome III indicating efficient crossover assurance. By contrast, 9.5% of *msh4–14KR* tetrads had zero crossovers ($p<0.001$ compared to wild type, *G* test). In addition, the fraction of tetrads with a single crossover increased from 11.1% in wild type to 40.1% in *msh4–14KR,* and multiple crossover classes decreased from 87.5 to 50.4% (Figure 2D and Supplemental Table S2). However, crossover assurance remained significantly more efficient in *msh4–14KR* cells than in the *msh4*Δ null mutant, which produced 24.5% non-exchange tetrads ($p<0.001$, *G* test).

The reduced efficiency of crossover assurance in *msh4–14KR* cells is expected to increase chromosome missegregation in the first meiotic division resulting in inviable gametes. Analysis of spore viability confirmed this prediction, revealing a significant increase in spore death in the *msh4–14KR* strain ($p<0.001$ relative to wild type, χ^2 test; Figure 2E and Supplemental Table S4) with a preponderance of tetrads containing two or zero viable spores, indicative of meiosis-I nondisjunction (Figure 2F). *msh4–14KR* spore viability was, however, much higher than that of the *msh4*Δ strain (72.9% versus 33.1%, $p<0.001$, χ^2 test), consistent with the more severe crossover assurance defect of the null mutant (Supplemental Table S4).

The SUMOylation defective *msh4–14KR* allele also caused defective crossover interference. Interference was assessed by analyzing coincident crossovers in adjacent genetic intervals

(Malkova et al., 2004)(Figure 2G and Supplemental Table S5). For each reference interval, tetrads were divided into two subsets: those with one or two detectable crossovers (tetratypes, TTs, and nonparental ditypes, NPDs i.e. double crossovers involving all four chromatids) and those without a crossover (parental ditypes, PDs). Map distances of the adjacent test interval were then analyzed for the two tetrad subsets and the ratio of the map distances was calculated (cM^{TT+NPD} / cM^{PD}). A ratio of significantly less than one indicates positive interference, i.e. coincident double crossovers occur less frequently than expected in the absence of interference. In wild-type, significant positive crossover interference was detected for all interval pairs except *LEU2–CEN3–MAT* on chromosome 3 (Figure 2G). Oppositely, the residual crossovers in *msh4*Δ cells did not show interference for any interval pairs. Four out of the six interval pairs analyzed lacked interference in *msh4–14KR* tetrads suggesting that interference is weakened but not completely abolished when Msh4 SUMOylation is defective. This inference was supported by analyzing frequencies of double crossovers within individual intervals (NPD ratios, Figure 2H and Supplemental Table S5). The ratio of observed NPD events over that expected in the absence of interference was calculated for each interval (Papazian, 1952; Stahl, 2008). Positive crossover interference, indicated by an NPD ratio of significantly less than one, was detected for all six intervals in wild type (NPD ratios ranged from 0.1 to 0.3). Significant interference was not detected for any interval in tetrads from either the *msh4*Δ null mutant or the SUMOylation-defective *msh4–14KR* strain. We conclude that SUMOylation of Msh4 facilitates the formation of crossovers that are subject to the patterning processes that result in crossover assurance and interference.

To confirm the importance of SUMOylation for Msh4 function, we asked whether the crossover defect of the *msh4–14KR* mutant could be rescued by directly fusing the Msh4–14KR protein to SUMO (Figure 3A, Supplemental Figure S6 and Table S4). C-terminal fusion of Msh4–14KR to a non-conjugatable form of SUMO (Smt3ΔGG) increased crossing over on chromosome III from 72.4% of wild-type levels in *msh4–14KR* cells to 88.4% in *msh4–14KR- SUMO* (Figure 3B). Moreover, the frequency of non-exchange chromosomes was reduced from 9.5% to 3.5% (Figure 3C; $p<0.001$, *G* test), and spore viability increased from 73% to 81% in *msh4–14KR* and *msh4–14KR-SUMO* strains, respectively ($p<0.01$, χ^2 test; Supplemental Figure S6 and Table S4), indicating improved crossover assurance (note that fusion of SUMO to wild-type Msh4 did not significantly impact crossing over or spore viability; *MSH4-SUMO* in Figure 3). Crossover interference was also partially restored, with 4/6 adjacent interval pairs showing significant positive interference in *msh4–14KR-SUMO* tetrads compared to 2/6 in *msh4–14KR* (Figure 3D). Restoration of interference was less conspicuous within genetic intervals, analyzed by NPD ratios, but significant positive interference was detected for 2/6 intervals in *msh4–14KR-SUMO* tetrads compared to 0/6 for *msh4–14KR* (Figure 3E).

In theory, the effects of SUMO fusion could be non-specific, for example by stabilizing Msh4–14KR. Therefore, we also analyzed a C-terminal fusion of Msh4–14KR to GFP, which is very stable in budding yeast and not subject to ubiquitin-mediated proteolysis (Supplemental Figure S6)(He et al., 2020). However, *msh4–14KR-GFP* did not rescue the crossover and spore viability defects seen in *msh4–14KR* cells. These data corroborate a specific role for SUMOylation in optimal Msh4 function.

Msh4 SUMOylation Promotes the Formation and Resolution of DNA Joint Molecules

To understand the role of Msh4 SUMOylation for the DNA steps of meiotic recombination, DNA intermediates were monitored via Southern blot at the *HIS4::LEU2* recombination hotspot in cultures undergoing synchronous meiosis (Figure 4)(Hunter and Kleckner, 2001; Oh et al., 2007). At this locus, restriction fragment polymorphisms between the two parental chromosomes (Mom and Dad) produce DNA fragments diagnostic for DSBs, JMs, crossover and noncrossover molecules (Figure 4A, and 4E,F). DSBs appeared and reached peak levels at similar time in cultures of wild-type, *msh4*Δ and *msh4–14KR* cells (Figure 4B,C). Relative to wild type, peak DSB levels were higher and DSBs turnover was delayed in both *msh4–14KR* and *msh4*Δ cells suggesting defective JM formation (below). Consonant with our genetic analysis of recombination, crossovers were reduced 1.6-fold in *msh4–14KR* cells, significantly less than the 2.9-fold reduction seen for *msh4*Δ cells at the *HIS4::LEU2* locus (Figure 4B,D). As seen previously (He et al., 2020), meiotic divisions were delayed by over 2 hrs in *msh4*Δ null mutants, while the *msh4–14KR* mutation caused only a ~30 min delay relative to wild type. Non-crossover levels measured at the *HIS4::LEU2* hotspot echoed gene conversion frequencies detected in tetrads with 1.4- and 2.3-fold increases seen in *msh4–14KR* and *msh4*Δ cells, respectively (Figure 4D).

Analysis of JM intermediates by 2D gels showed that Msh4 SUMOylation facilitates the formation and resolution of JM intermediates (Figure 4E–H). In *msh4–14KR* cells, the formation and disappearance of all JM species was delayed relative to wild-type by ~30–45 mins (Figure 4G) and average peak levels of the different JM species were reduced 1.3- to 2.8-fold relative to wild type (Figure 4H). *msh4*Δ cells showed similar delays in the formation and resolution of JMs, but average peak levels were more severely reduced (2.3- to 6.7-fold). Thus, Msh4 SUMOylation is required for full functionality of MutSγ with respect to the formation of JMs and their resolution into crossovers.

Msh4 SUMOylation Facilitates Homolog Synapsis

The elevated frequency of gene conversion in *msh4–14KR* cells is a signature of defective homolog engagement in *zmm* mutants (Thacker et al., 2014). This observation, together with delayed and inefficient JM formation caused by the *msh4–14KR* allele, led us to ask whether homolog synapsis was also defective in this mutant. Synapsis was monitored by immuno-staining spread chromosomes for Zip1, the major component of synaptonemal complex (SC) central region (Figure 5). Nuclei were assigned to one of three classes based on the extent of Zip1 staining (Borner et al., 2004): class I nuclei contained only dotty Zip1 structures; class II nuclei had partial synapsis with both linear and dotty Zip1 staining; and class III had continuous Zip1 lines indicative of the full synapsis seen in the pachytene stage (Figure 5A). Nuclei were also analyzed for the presence of polycomplexes, large extrachromosomal assemblies of Zip1 indicative of synapsis defects (Sym and Roeder, 1995).

In wild-type nuclei, synapsis was well underway by 4 hrs, peak levels of class III nuclei (35%) were seen at 5 hrs and Zip1 staining had largely disappeared by 8 hrs indicative of SC disassembly (Figure 5B). Synapsis was less efficient in *msh4–14KR* nuclei with lower peak levels of class III nuclei (23%) emerging an hour later than in wild type ($p<0.05$ relative to wild-type, *G* test). Consistent with an SC defect in *msh4–14KR* nuclei, polycomplexes were

present in up to 52% of nuclei compared to a maximum of 21% in wild-type. However, synapsis in *msh4*Δ null mutant nuclei was much more defective than in *msh4–14KR,* with the peak level of class III nuclei reaching only 9% and polycomplexes forming in 68% of nuclei ($p<0.05$, *G* test).

Chromosomal Localization of Msh4 Is Enhanced By SUMOylation

SUMOylation can regulate protein function in a number of ways including mediating protein-protein interactions, altering protein stability and promoting subcellular protein localization (Flotho and Melchior, 2013; Gareau and Lima, 2010). As a first step to ascertain how SUMOylation enhances Msh4 function, we monitored the chromosomal localization of the SUMOylation-defective Msh4–14KR protein and wild-type Msh4 by immunostaining surface spread nuclei. Numbers of Msh4 immunostaining foci were quantified in nuclei with zygotene (class II) and pachytene (class III) morphologies, i.e. partial and complete lines of Zip1 staining (Figure 5C and 5D; analysis of full time-courses is shown in Supplemental Figure S7). In wild-type, Msh4 foci averaged 43.9 ± 13.3 S.D. per nucleus while focus numbers in *msh4–14KR* nuclei were significantly lower, averaging 35.5 ± 10.9 S.D. ($p<0.005$, *t* test; Figure 5D). Thus, SUMOylation of Msh4 somehow enhances its chromosomal localization.

SUMOylation Does Not Function To Stabilize Msh4

The reduced chromosomal localization of Msh4–14KR could be explained if SUMOylation stabilized the Msh4 protein, for example by antagonizing proteasomal proteolysis. Under this model, SUMO may function in the same pathway as phosphorylation, which counteracts a degron moiety in the N-terminus of Msh4 and is essential for its crossover function (He et al., 2020). Alternatively, SUMOylation could promote chromosomal localization of Msh4 in some other way such as mediating interactions with partner proteins or enhancing binding to JMs. To begin to distinguish these possibilities, Msh4 and Msh4–14KR protein levels were analyzed throughout meiosis via Western blotting (Figure 6A). Msh4 and Msh4–14KR protein levels were very similar at all timepoints (Figure 6B) indicating that SUMOylation does not promote Msh4 function by enhancing its stability; and further implying that SUMOylation acts independently of the DDK (Dbf4-dependent kinase Cdc7)-mediated phosphorylation pathway that activates the crossover function of Msh4 by attenuating its proteasomal proteolysis (He et al., 2020). Consistently, phosphorylated levels did not differ between Msh4 and Msh4–14KR samples (Figure 6C, quantification of the slower-migrating phosphorylated isoform of Msh4).

SUMOylation of Msh4 Enhances Its Interaction With Msh5

As Msh4 functions as an obligate heterodimer with Msh5, we examined whether SUMOylation influences this interaction. To this end, Msh5 was immunoprecipitated from meiotic cultures of *MSH4* (wild type) and *msh4–14KR* strains and the relative amounts of Msh4 or Msh4–14KR that co-immunoprecipitated was quantified (Figure 6D–E). Input samples from the two strains contained identical levels of Msh4 and Msh5; and in both cases identical amounts of Msh5 were immunoprecipitated. However, the amount of SUMOylation-defective Msh4–14KR protein that co-immunoprecipitated with Msh5 was ~32% lower than that seen for wild-type Msh4 (Figure 6E and 6F). We infer that

SUMOylation of Msh4 fosters the interaction between Msh4 and Msh5 to facilitate assembly of the MutSγ complex. Consistent with this interpretation, the Msh4–14KR-SUMO fusion partially rescued the Msh5 interaction defect of Msh4–14KR (Figure 6D,E).

Msh4 SUMOylation Requires DSB Formation But Not Downstream Steps Of Meiotic Recombination

The relationships between Msh4 SUMOylation and the events of meiotic prophase were determined by analyzing a panel of mutants defective for successive steps of meiotic recombination and homolog synapsis, namely: DSB formation (*spo11-Y135F*); the 5' resection of DSB ends *(sae2*Δ*);* homologous pairing and DNA strand exchange *(mnd1*Δ*);* synaptonemal complex formation *(zip1*Δ*);* exit from pachytene, including desynapsis and the resolution of dHJs into crossovers *(ndt80*Δ*);* and the crossover biased resolution of dHJs (*mlh3*Δ)(Figure 7A). We also further examined the relationship between the SUMOylation of Msh4 and its stabilization by phosphorylation by analyzing a strain carrying the phosphorylation-defective *msh4–6A* allele (He et al., 2020). For each strain, Msh4 was immunoprecipitated and analyzed by Western blotting for SUMO. SUMOylated Msh4 was detected in all mutant strains with one exception, *spo11- Y135F* (Figure 7B). These observations have three important implications: (i) unresected DSBs are sufficient to trigger Msh4 SUMOylation; (ii) in contrast to phosphorylation (He et al., 2020), modification of Msh4 by SUMO does not require MutSγ to engage JM intermediates; and (iii), consistent with (ii), SUMOylation of Msh4 occurs independently of its phosphorylation (and *vice versa,* see Figure 6C).

The DSB dependence of Msh4 SUMOylation predicts that Msh4-Msh5 interaction will be reduced in DSB-defective *spo11-Y135F* cells. Co-immunoprecipitation experiments confirmed this prediction (Figure 7C and Supplemental Figure S8A). In *spo11-Y135F* cells, the amount of Msh4 that co-immunoprecipitated with Msh5 was 37% lower than in wild-type cells, and *spo11-Y135F* and *msh4–14KR* mutations were epistatic for reduced Msh4-Msh5 interaction. A caveat to this experiment is that Msh4 levels are reduced in *spo11-Y135F* cells because its N-terminal degron is not phosphorylated (He et al., 2020) (Supplemental Figure S8). To confirm that DSB-dependent SUMOylation functions independently of phosphorylation-dependent stabilization, Msh4-Msh5 interaction was analyzed in *msh4–6D* cells expressing a stable phosphomimetic allele of Msh4 (Figure 7D and Supplemental Figure S8B). Input controls showed that levels of the Msh4–6D protein were identical in wild-type and *spo11-Y135F* cells (Supplemental Figure S8B). However, Msh4-Msh5 interaction remained defective in the absence of DSBs, with 37% less Msh4 co-immunoprecipitating with Msh5 in *msh4–6D spo11-Y135F* cells (Figure 7D). Thus, DSB-dependent SUMOylation of Msh4 mediates the efficient assembly of MutSγ complexes.

Notably, only a single, mono-SUMOylated form of Msh4 was detected in *sae2*Δ*, mnd1*Δ and *zip1*Δ strains, while higher molecular-weight species were detectable in other strains (marked by white dots in Figure 7B). The genetic requirements for the larger SUMOylated forms match those required for Msh4 phosphorylation (He et al., 2020) suggesting that these species could be co-modified by SUMO and phosphorylation. Accumulation of the larger SUMOylated species in *ndt80*Δ cells, in which phosphorylated Msh4 accumulates to high

levels (He et al., 2020), could be consistent this possibility. However, the presence of larger SUMOylated forms in phosphorylation-defective *msh4–6A* cells argues against this interpretation, instead suggesting that Msh4 becomes multi-/poly-SUMOylated following homolog engagement (see below).

Given that Ubc9 can directly SUMOylate Msh4 *in vitro* (Figure 1B,C) we also analyzed the *in vivo* requirements for the four known budding yeast SUMO E3-ligases, Siz1, Siz2, Mms21 and the meiosis-specific Zip3 (Figure 7C). In *siz1*Δ *A, siz2* Δ and *zip3*Δ null mutants, a *siz1*Δ *siz2*Δ double mutant and the ligase-defective *mms21–11* mutant, Msh4 SUMOylation was still detected (Figure 7C) consistent with Msh4 being a direct target of Ubc9 *in vivo,* as seen *in vitro* (Figure 1B and 1C). Notably, only mono-SUMOylated Msh4 was detected in *zip3*Δ cells, while larger SUMOylated species were detected in the other ligase mutants. This observation allowed us to further test the interpretation that Msh4 becomes multi-/poly-SUMOylated following homolog engagement. Xaver et al. showed that *mms21–11* mutation partially suppresses the severe chromosome pairing defect of *zip3*Δ cells, enabling pseudo-synapsis in which homologs are paired and intimately connected at discrete axial associations (Xaver et al., 2013). IP Western analysis of Msh4 from a *zip3*Δ *mms21–11* double mutant revealed the presence of multi-/poly-SUMOylated forms, although Msh4 phosphorylation was not restored. Thus, Msh4 appears to undergo a two stage SUMOylation process, becoming mono-SUMOylated in response to DSB formation and then multi-/poly-SUMOylated following DNA strand-exchange and homolog pairing.

DISCUSSION

Msh4 Is A Hub For Crossover Regulation

We recently described a pathway of crossover regulation that governs the stability of Msh4 (He et al., 2020). Msh4 is intrinsically unstable by virtue of an N-terminal degron moiety that directly mediates its proteasomal proteolysis. Following homolog engagement, phosphorylation by the Dbf4-dependent kinase, Cdc7, attenuates the degron to stabilize Msh4 and thereby enables the crossover function of MutSγ. The current study defines a distinct pathway of crossover regulation that also targets Msh4. Initial Msh4 SUMOylation occurs prior to its phosphorylation and requires DSB formation but not subsequent steps of recombination. Further modification leading to multi/poly-SUMOylated Msh4 requires homolog engagement but also occurs independently of phosphorylation (Figure 7B). Thus, Msh4 is a hub for crossover regulation by two independent pathways (SUMO and phosphorylation) that act successively via two distinct mechanisms (Msh4-Msh5 interaction and Msh4 stability) to constrain the activity of MutSγ in space and time.

SUMO Augments Msh4-Msh5 Interaction

Msh4 SUMOylation represents a context-dependent enhancement of MutSγ function that increases the efficiency of crossover assurance to ensure faithful chromosome segregation during meiosis. SUMO is not required for Msh4 and Msh5 to interact *per se* but clearly augments this interaction to increase steady-state levels of the MutSγ complex. Why MutSγ is regulated in this way remains unclear. The DSB dependence of Msh4-SUMOylation suggests that it may be important to limit the availability of stable MutSγ complexes prior to

DSB formation and when DSB levels are low, which could help minimize deleterious binding to replication- related DNA structures and non-productive stabilization of early occurring strand-exchange intermediates that form before interhomolog bias is efficiently enforced (Joshi et al., 2015). Subsequently, with increasing DSB levels, Msh4-SUMOylation could act as a rheostat that helps deliver optimal levels of MutSγ complexes as homolog engagement ensues.

More generally, in the absence Msh4 SUMOylation, the apo-MutSγ complex may be intrinsically unstable, for example until nucleotide is bound. Under this scenario, reduced Msh4- Msh5 interaction is a readout of this suboptimal conformation. Another non-exclusive possibility is that the MutSγ structure must be very flexible to enable JM binding and conformational changes, such as those inferred to occur upon nucleotide exchange and hydrolysis (Snowden et al., 2008), but that the requisite dynamicity renders MutSγ prone to fall apart. Like most SUMO targets, the steady-state fraction of Msh4 that is modified is low (discrete SUMOylated forms were not readily detected by Western analysis of whole-cell extracts). Thus, enhancement of MutSγ complex formation must be mediated by transient modification of Msh4. Possibly, Msh4-SUMOylation is required only for initial Msh4-Msh5 interaction, but not thereafter; alternatively, SUMOylation could help overcome an energy barrier to stable Msh4-Msh5 interaction; or it could act to prevent alternative interactions such as Msh4 self-interaction or interaction with a chaperone.

Interaction between SUMO and SUMO-interacting motifs (SIMs)(Gareau and Lima, 2010; Sekiyama et al., 2008) is one way in which Msh4-SUMOylation could facilitate interaction with Msh5. Indeed, Msh5 contains a number of candidate SIMs that could interact with SUMOylated Msh4 (Supplemental Figure S3). However, we have not been able to demonstrate a clear role for the Msh5 SIMs in Msh4-Msh5 interaction and, as described above, this is not the only way in which Msh4 SUMOylation might enhance the assembly of MutSγ

Ubc9 Can Directly SUMOylate Msh4

Msh4 appears to be a direct substrate of the E2 conjugase, Ubc9. *In vivo,* SUMOylation of Msh4 occurs independently of the four known SUMO E3 ligases (in *siz1*Δ*, siz2*Δ*, zip3*Δ and *mms21–11* single mutants; and in *siz1*Δ *siz2*Δ and *zip3*Δ *mms21–11* double mutants; Figure 7E). Although it is formally possible that all four ligases are redundant for targeting Msh4, our *in vitro* analysis showed that Ubc9 directly and specifically SUMOylates Msh4, but not Msh5 (Figure 1B,C). Ubc9 directly binds the consensus SUMOylation peptide, Ψ-K-x-E/D (Ψ = large hydrophobic residue), to favor modification at these sites (Bernier-Villamor et al., 2002). Surprisingly, none of the mapped Msh4 SUMOylation sites match this or other defined consensus motifs. Indeed, several consensus SUMOylation sites (at lysines 128, 185, 281, 330, 365, 445 and 463) were not modified. This raises the question of how Ubc9 directly targets Msh4. One possibility is that Ubc9 specificity is altered or generally relaxed during meiosis. Consistent with this possibility, a majority of the more than 2,700 SUMO sites mapped during meiosis in budding yeast have no recognizable motif (Bhagwat et al., 2021). Another possibility is that Msh4 (or the MutSγ complex) interacts with Ubc9 in some other way, via a dedicated binding site and/or SIMs, and acts as an auto-E3 or E3-like

cofactor for Ubc9 catalysis, similar to the DNA-repair nuclease platform, SLX4 (Guervilly et al., 2015).

DSB-Dependent Msh4 SUMOylation Anticipates Joint Molecule Formation.

DSB-induced SUMOylation of Msh4 represents a previously unknown pathway that couples the initiation of meiotic recombination to downstream events of crossover control. Mono-SUMOylation of Msh4 requires the formation of DSBs but not their resection. Indeed, Msh4 SUMOylation is not obviously changed even when resected DSBs accumulate, as in the *mnd1*Δ mutant (Figure 7B). This contrasts the DNA-damage induced SUMOylation characterized in mitotically cycling cells, which is largely dependent on the resection machinery and a pathway involving an ensemble of ssDNA, RPA and the E3 ligase Siz2 (Chung and Zhao, 2015; Dhingra and Zhao, 2019). Perhaps the large numbers of programmed DSBs (~200) formed during meiosis are sufficient to maximally activate SUMOylation without the need for the signaling platform afforded by ssDNA. The implications are that initial Msh4 SUMOylation does not conform to the “on-site” SUMOylation paradigm, in which DNA metabolism factors are modified only once they have engaged DNA or chromatin (Dhingra and Zhao, 2019), and that it is triggered by an as yet uncharacterized DSB-signaling pathway. It will be interesting to learn the nature of this pathway and to see if meiotic DSBs trigger a wave of target SUMOylations in addition to Msh4.

Homolog Engagement Licenses Secondary SUMOylation of Msh4

Multi/poly-SUMOylation of Msh4 requires JM formation and other factors known to be important for MutSγ to efficiently load at recombination sites, such as the SC protein Zip1 and SUMO ligase Zip3 (Figure 7B and 7E). In this regard, secondary SUMOylation of Msh4 resembles canonical “on site” modification (Dhingra and Zhao, 2019). However, unlike DNA-damage induced SUMOylation, Msh4 multi/poly-SUMOylation does not require Siz2 implying the involvement of another distinct, possibly meiosis-specific pathway. Notably, Zip3 and Ubc9 colocalize at nascent sites of homolog synapsis sites and both Zip1 and Zip3 are required for Ubc9 localization along SCs (Hooker and Roeder, 2006). Although Zip3 was not required for Msh4 SUMOylation *in vitro,* it did generally stimulate the reaction (Figure 1B). Possibly, a Zip1- Zip3 ensemble indirectly targets secondary SUMOylation of Msh4 at recombination sites by locally recruiting Ubc9. Importantly, the requirement for Zip3 in Msh4 multi/poly-SUMOylation can be bypassed by the *mms21–11* mutation (Figure 7G) suggesting a constraining function of Mms21-catalyzed SUMOylation of currently unknown targets.

Msh4 SUMOylation clearly continues after dHJs have formed during pachytene, exemplified by the accumulation of modified forms in *ndt80*Δ cells (Figure 7B). Multi/poly-SUMOylation of Msh4 might be an innocuous readout of MutSγ complexes that are engaged in recombination and protected from de-SUMOylating isopeptidases. A more active role for continued SUMOylation could be to locally enhance levels of MutSγ in order to stabilize dHJs and maintain their crossover fate. Presumably, the continued integrity of MutSγ complexes is also required to help trigger crossover-specific dHJ resolution mediated by the endonuclease MutLγ (Cannavo et al., 2020; Kulkarni et al., 2020; Zakharyevich et

al., 2012). Multi/poly-SUMOylation of Msh4 could further stabilize Msh4-Msh5 interaction; promote accumulation of MutSγ at prospective crossover sites; or help engage resolution factors via SUMO-SIM interactions.

Limitations Of The Study

Our study identifies a pathway of meiotic crossover regulation through DSB-dependent SUMOylation of Msh4 that has distinct features relative to the DNA-damage triggered SUMOylation pathways characterized in mitotically cycling cells (Chung and Zhao, 2015; Dhingra and Zhao, 2019). Although there is a clear correlation between levels of MutSγ and crossing over (this study and (He et al., 2020) we cannot tell whether the reduced level of MutSγ in SUMOylation-defective *msh4–14KR* cells is the sole cause of reduced crossing over in this mutant; a likely possibility is that the activity of residual MutSγ complexes is also compromised. Furthermore, we cannot yet distinguish the contributions of mono-versus multi/poly- SUMOylation of Msh4 to crossover control. Exactly how Msh4-SUMOylation augments the function of MutSγ also remains unclear and further studies must address possibilities such as promoting SUMO-SIM interactions between Msh4 and Msh5, or between Msh4 and other proteins; disrupting self-interaction of Msh4 or interaction between Msh4 and another factor such as a chaperone; enhancing nuclear localization of Msh4; or facilitating a conformational change required to stabilize MutSγ. Finally, it remains unclear why MutSγ is regulated in this way and whether this pathway is conserved in other species.

STAR★Methods

RESOURCE AVAILABILITY

Lead contact—Further information and requests for resources and reagents should be directed to and will be fulfilled by the Lead Contact Neil Hunter, nhunter@ucdavis.edu

Materials availability—Plasmids generated in this study will be provided upon request.

Data and code availability—This study did not generate/analyze datasets/code.

EXPERIMENTAL MODEL AND SUBJECT DETAILS

The genotypes of the diploid *Saccharomyces cerevisiae* strains (SK1 background) used in this study are listed in Table S7.

Synthetic dropout and YPD solid and liquid media were prepared according to standard protocols (Owens et al., 2018; Sherman, 2002). SPS and SPM media for meiotic time courses were prepared as described (Owens et al., 2018). All yeast cultures were incubated at 30°C.

METHOD DETAILS

Yeast Strains—All strains are derivative of strain SK1 and listed in Table S7. The primers used for mutagenesis are listed in Table S6.

Meiotic Time Courses and DNA Physical Assays—Meiotic time course and DNA physical assays were performed as previously described (Owens et al., 2018). Briefly, synchronous yeast cultures were induced to undergo meiosis in sporulation media, samples were taken over time to monitor the meiotic recombination events. Recombination events at HIS4::LEU2 locus were monitored by gel electrophoresis. The HIS4::LEU2 assay system contains XhoI restriction site polymorphisms between parental homologs producing fragments diagnostic for parental and recombinant chromosomes. A BamHI/NgoMIV polymorphism immediately at the DSB site allows detection of non-crossover products on one-dimensional gels. Meiotic progression was analyzed by counting the numbers of DAPI staining bodies per cell in samples fixed in 40% ethanol, 0.1 M sorbitol. At least 100 cells were counted per time point. Error bars represent averages (± SD) from three or four experiments.

Tetrad Analysis—Haploid strains were mated for 6 hrs on YPD plates and sporulated on plates containing 1% potassium acetate at 30°C for two days. Tetrad analysis was performed using standard techniques as described (Perkins, 1949). Map distances and NPD ratios were calculated using Stahl Lab Online Tools (http://elizabethhousworth.com/StahlLabOnlineTools/). *MSH4* SUMOylation site alleles were created by using QuikChange II Site-Directed Mutagenesis Kit (Agilent Technologies Inc, 200524) and confirmed by DNA sequencing (GENEWIZ). All alleles were sequenced in their entirety to ensure that no additional mutations were introduced.

Protein Analysis by Western Blotting—TCA extractions were performed as described (Johnson and Blobel, 1999). Samples were analyzed by standard SDS-PAGE and Western analysis. Primary antibodies targeting the following tags or proteins were used: mouse anti-HA (12CA5) (1:2,000, Millipore Sigma), rabbit anti-Smt3 (1:500, a gift from Dr. Steve Brill), Arp7 (1:10,000, Santa Cruz, SC-8960), anti-Msh4 and anti-Msh5 (1:500, a gift from Dr. Akira Shinohara). Secondary antibodies (1:10,000) were IRDye® 800CW Donkey anti-Mouse IgG (LI-COR, 925–32212), IRDye® 680LT Donkey anti-Goat IgG (LI-COR, 925–68024), IRDye® 680LT Donkey anti-Rabbit IgG (LI-COR, 925–68023) and IRDye® 800CW Donkey anti-Rabbit IgG (LI-COR, 925–32213). Western blots were imaged on an Odyssey Infrared Imager (LI-COR) and quantification of protein bands was performed using Image Studio Lite Ver 4.0 software.

Protein Purifications—The plasmids pET15b-Aos1, pET28b-Uba2 and pET28b-Ubc9 were a kind gift from Dr. Christopher Lima (MSKCC)(Yunus and Lima, 2009). The plasmid pET28b-Smt3-KallR was generated by mutating all lysines in Smt3 to arginine in plasmid pET28b-Smt3 (a generous gift from Dr. Steve Brill, Rutgers University)(Mullen and Brill, 2008). Purification of proteins Aos1, Uba2, Ubc9 and Smt3 were performed as described previously (Yunus and Lima, 2009). pFB-MSH4-strep and pFB-MSH5-his and purification of the *S. cerevisiae* MutSγ complex from Sf9 cells have been described (He et al., 2020). The *ZIP3* gene was amplified from *S. cerevisiae* SK1 genomic DNA with a C-terminal Strep tag and cloned into the NcoI and NheI sites of pET28b (Novagen) to create pET28b-Zip3-Strep. The construct was transformed into ArcticExpress (DE3) cells, a single colony was grown to saturation in LB medium, and the culture was diluted 100-fold into LB medium

containing 1% glucose, 1% glycerol, 1 mM $MgSO_4$ and 1 mM $ZnSO_4$, and grown at 30°C with shaking at 250 rpm until the optical density at 600 nm reached ~0.4. After cooling the culture to 11°C, protein expression was induced with 0.05 mM isopropyl-1-thio-α-d-galctopyranoside (IPTG) for 24 hours. Cells were harvested and lysed in lysate buffer (50 mM Tris-HCl pH 8.0, 0.2% (w/v) Triton X-100, 400 mM NaCl, 0.1 mM $ZnCl_2$, 10% glycerol and 5 mM TCEP) using a microfluidizer. The cell lysate was applied to a 1 ml StrepTrap HP column and the Zip3-Strep was eluted with lysate buffer containing 2.5 mM desthiobiotin. Zip3-Strep was further enriched by S-100 gel filtration column, quantified using the bicinchonic acid (BCA) assay, and stored in aliquots at −80°C.

In Vitro SUMOylation—*In vitro* SUMOylation reactions were performed at 30°C for 1 hr in a reaction mixture containing 20 mM HEPES (pH7.5), 50 mM NaCl, 0.1% Tween-20, 1 mM DTT, 200 nM yeast E1 (Uba2-Aos1), 100 nM of yeast E2 (Ubc9), 80 μM Smt3-KallR (with all lysines substituted by arginine), 4 μM of yeast Msh4-Msh5, 2 mM $MgCl_2$, 2 mM ATP and ± 100 nM Zip3. In negative controls, 2 mM EDTA was added. The reactions were stopped by adding 6x Laemmli buffer, resolved by SDS-PAGE (8% polyacrylamide) and visualized by western blot using anti-Msh4 and anti-Msh5 antibodies, respectively.

LC-MS/MS Analysis—Protein samples in gel slices were digested with trypsin overnight at 25°C. Peptide were cleaned up using a MacroSpin column (The Next Group). The peptides were then separated using a Proxeon Easy-nLC II HPLC (Thermo Scientific) and analyzed on a Q Exactive Orbitrap mass spectrometer with a Proxeon nanospray source (Thermo). The collected spectra and fragmentation profiles were searched against a Uniprot *Saccharomyces cerevisiae* proteome database. Peptide matches were analyzed using Scaffold4.

Immunofluorescence microscopy—Chromosome spreads were processed for immunostaining as described previously (Grubb et al., 2015; Loidl and Lorenz, 2009) using the following antibodies: mouse anti-HA antibody (Millipore Sigma; 11583816001, 1:200) and rabbit anti-Zip1 antibody (a gift from Dr. Akira Shinohara, 1:200). Goat secondary antibodies (anti-rabbit 568, A11036; and anti-mouse 488, A11029) were conjugated to Alexa 568 and Alexa 488 (Molecular Probes, 1:1000). Coverslips were mounted with Prolong Gold antifade reagent (Invitrogen P36930). Digital images were acquired using a Zeiss AxioPlan II microscope, Hamamatsu ORCA-ER CCD camera and analyzed using Volocity software. Scatterplots were generated using the Graphpad program in Prism.

Co-immunoprecipitation of MutSγ complexes—Indicated strains carrying C-terminally tagged Msh4–3xHA and Msh5–3xFLAG were induced to undergo meiosis. Cells from 50 mL samples were harvested after 6 hrs, washed with dH_2O and snap-frozen in liquid nitrogen. Frozen cells were ground in a FreezerMill Cryogenic Grinder (SPEX SamplePrep, 6970EFM) and the cell powder was incubated with an equal volume of lysis buffer (50 mM HEPES-KOH pH 7.8, 150 mM KCl, 1 mM EDTA, 10% glycerol, 0.005% NP- 40, 0.05% Tween-20, 1X complete™ Protease Inhibitor Cocktail (Millipore Sigma 11697498001) for 2 hrs at 4°C. The cell extract was clarified by centrifugation for 1 hr at 40,000g and the supernatant incubated with 30 μl of anti-FLAG M2 Magnetic Beads (Sigma

Aldrich, M8823) for 4 hrs at 4°C. Beads were then washed five time with lysis buffer. Immuno-precipitated proteins were then eluted by boiling in 20 μl of 2X Laemmli buffer for 5 min and analyzed by Western blotting.

Molecular modeling—The homology model of the heterodimer was generated from a structure-based sequence alignment of the MutS family of proteins with known X-ray crystal structures as described (Lahiri, 2019); and images were rendered using the Molecular Visualization program, Pymol (https://pymol.org/2/). Potential SIMs on Msh5 were identified using the prediction tool JASSA (Joined Advanced Sumoylation Site and SIM Analyzer)(Beauclair et al., 2015) and manual examination of the *S. cerevisiae* Msh5 amino acid sequence.

QUANTIFICATION AND STATISTICAL ANALYSIS

Most data are presented as means ± SEM or SD and represent at least three independent experiments. Statistical tests, *p* and *n* values are described in the figures and figure legends

Supplementary Material

Refer to Web version on PubMed Central for supplementary material.

ACKNOWLEDGEMENTS

We thank Christopher Lima (MSKCC), Petr Cejka, Steve Brill (Rutgers University), Angelika Amon (Massachusetts Institute of Technology) and Akira Shinohara (Osaka University) for reagents, Darren Weber and Brett Phinney at UC Davis Proteomics Core and members of the Hunter Lab for support and discussions. This work was supported by NIH NIGMS grants GM074223 to N.H. and R15 GM135904 to I.M. N.H. is an Investigator of the Howard Hughes Medical Institute.

REFERENCES

Allers T, and Lichten M (2001). Differential timing and control of noncrossover and crossover recombination during meiosis. Cell 106, 47–57. [PubMed: 11461701]

Almedawar S, Colomina N, Bermudez-Lopez M, Pocino-Merino I, and Torres-Rosell J (2012). A SUMO-dependent step during establishment of sister chromatid cohesion. Current biology : CB 22, 1576–1581. [PubMed: 22771040]

Arora K, and Corbett KD (2019). The conserved XPF:ERCC1-like Zip2:Spo16 complex controls meiotic crossover formation through structure-specific DNA binding. Nucleic acids research 47, 2365–2376. [PubMed: 30566683]

Beauclair G, Bridier-Nahmias A, Zagury JF, Saib A, and Zamborlini A (2015). JASSA: a comprehensive tool for prediction of SUMOylation sites and SIMs. Bioinformatics 31, 3483–3491. [PubMed: 26142185]

Bernier-Villamor V, Sampson DA, Matunis MJ, and Lima CD (2002). Structural basis for E2-mediated SUMO conjugation revealed by a complex between ubiquitin-conjugating enzyme Ubc9 and RanGAP1. Cell 108, 345–356. [PubMed: 11853669]

Bhagwat NR, Owens SN, Ito M, Boinapalli JV, Poa P, Ditzel A, Kopparapu S, Mahalawat M, Davies OR, Collins SR, et al. (2021). SUMO is a pervasive regulator of meiosis. eLife 10.

Borner GV, Kleckner N, and Hunter N (2004). Crossover/noncrossover differentiation, synaptonemal complex formation, and regulatory surveillance at the leptotene/zygotene transition of meiosis. Cell 117, 29–45. [PubMed: 15066280]

Brown MS, and Bishop DK (2014). DNA strand exchange and RecA homologs in meiosis. Cold Spring Harbor perspectives in biology 7, a016659. [PubMed: 25475089]

Cannavo E, Sanchez A, Anand R, Ranjha L, Hugener J, Adam C, Acharya A, Weyland N, Aran-Guiu X, Charbonnier JB, et al. (2020). Regulation of the MLH1-MLH3 endonuclease in meiosis. Nature.

Chan LY, and Amon A (2010). Spindle position is coordinated with cell-cycle progression through establishment of mitotic exit-activating and -inhibitory zones. Mol Cell 39, 444–454. [PubMed: 20705245]

Chen C, Zhang W, Timofejeva L, Gerardin Y, and Ma H (2005). The Arabidopsis ROCK- N-ROLLERS gene encodes a homolog of the yeast ATP-dependent DNA helicase MER3 and is required for normal meiotic crossover formation. Plant J 43, 321–334. [PubMed: 16045469]

Cheng CH, Lo YH, Liang SS, Ti SC, Lin FM, Yeh CH, Huang HY, and Wang TF (2006). SUMO modifications control assembly of synaptonemal complex and polycomplex in meiosis of Saccharomyces cerevisiae. Genes & development 20, 2067–2081. [PubMed: 16847351]

Chung I, and Zhao X (2015). DNA break-induced sumoylation is enabled by collaboration between a SUMO ligase and the ssDNA-binding complex RPA. Genes & development 29, 1593–1598. [PubMed: 26253534]

De Muyt A, Pyatnitskaya A, Andreani J, Ranjha L, Ramus C, Laureau R, Fernandez- Vega A, Holoch D, Girard E, Govin J, et al. (2018). A meiotic XPF-ERCC1-like complex recognizes joint molecule recombination intermediates to promote crossover formation. Genes & development 32, 283–296. [PubMed: 29440262]

Dhingra N, and Zhao X (2019). Intricate SUMO-based control of the homologous recombination machinery. Genes & development 33, 1346–1354. [PubMed: 31575678]

Duroc Y, Kumar R, Ranjha L, Adam C, Guerois R, Md Muntaz K, Marsolier-Kergoat MC, Dingli F, Laureau R, Loew D, et al. (2017). Concerted action of the MutLbeta heterodimer and Mer3 helicase regulates the global extent of meiotic gene conversion. eLife 6.

Flotho A, and Melchior F (2013). Sumoylation: a regulatory protein modification in health and disease. Annual review of biochemistry 82, 357–385.

Gareau JR, and Lima CD (2010). The SUMO pathway: emerging mechanisms that shape specificity, conjugation and recognition. Nature reviews. Molecular cell biology 11, 861–871. [PubMed: 21102611]

Grubb J, Brown MS, and Bishop DK (2015). Surface Spreading and Immunostaining of Yeast Chromosomes. J Vis Exp, e53081. [PubMed: 26325523]

Guervilly JH, Takedachi A, Naim V, Scaglione S, Chawhan C, Lovera Y, Despras E, Kuraoka I, Kannouche P, Rosselli F, et al. (2015). The SLX4 complex is a SUMO E3 ligase that impacts on replication stress outcome and genome stability. Molecular cell 57, 123–137. [PubMed: 25533188]

Guiraldelli MF, Eyster C, Wilkerson JL, Dresser ME, and Pezza RJ (2013). Mouse HFM1/Mer3 is required for crossover formation and complete synapsis of homologous chromosomes during meiosis. PLoS genetics 9, e1003383. [PubMed: 23555294]

Guiraldelli MF, Felberg A, Almeida LP, Parikh A, de Castro RO, and Pezza RJ (2018). SHOC1 is a ERCC4-(HhH)2-like protein, integral to the formation of crossover recombination intermediates during mammalian meiosis. PLoS genetics 14, e1007381. [PubMed: 29742103]

He W, Rao H, Tang S, Bhagwat N, Kulkarni DS, Ma Y, Chang MAW, Hall C, Bragg JW, Manasca HS, et al. (2020). Regulated Proteolysis of MutSgamma Controls Meiotic Crossing Over. Molecular cell 78, 168–183 e165. [PubMed: 32130890]

Henderson KA, and Keeney S (2004). Tying synaptonemal complex initiation to the formation and programmed repair of DNA double-strand breaks. Proceedings of the National Academy of Sciences of the United States of America 101, 4519–4524. [PubMed: 15070750]

Herbert M, Kalleas D, Cooney D, Lamb M, and Lister L (2015). Meiosis and maternal aging: insights from aneuploid oocytes and trisomy births. Cold Spring Harbor perspectives in biology 7, a017970. [PubMed: 25833844]

Hooker GW, and Roeder GS (2006). A Role for SUMO in meiotic chromosome synapsis. Current biology : CB 16, 1238–1243. [PubMed: 16782016]

Hunter N (2015). Meiotic Recombination: The Essence of Heredity. Cold Spring Harbor perspectives in biology 7.

Hunter N, and Kleckner N (2001). The single-end invasion: an asymmetric intermediate at the double-strand break to double-holliday junction transition of meiotic recombination. Cell 106, 59–70. [PubMed: 11461702]

Jentsch S, and Psakhye I (2013). Control of nuclear activities by substrate-selective and protein-group SUMOylation. Annual review of genetics 47, 167–186.

Johnson ES, and Blobel G (1999). Cell cycle-regulated attachment of the ubiquitin-related protein SUMO to the yeast septins. The Journal of cell biology 147, 981–994. [PubMed: 10579719]

Joshi N, Brown MS, Bishop DK, and Borner GV (2015). Gradual implementation of the meiotic recombination program via checkpoint pathways controlled by global DSB levels. Molecular cell 57, 797–811. [PubMed: 25661491]

Kerscher O, Felberbaum R, and Hochstrasser M (2006). Modification of proteins by ubiquitin and ubiquitin-like proteins. Annu Rev Cell Dev Biol 22, 159–180. [PubMed: 16753028]

Kim S, Peterson SE, Jasin M, and Keeney S (2016). Mechanisms of germ line genome instability. Semin Cell Dev Biol 54, 177–187. [PubMed: 26880205]

Kulkarni DS, Owens SN, Honda M, Ito M, Yang Y, Corrigan MW, Chen L, Quan AL, and Hunter N (2020). PCNA activates the MutLgamma endonuclease to promote meiotic crossing over. Nature.

Lahiri S (2019). Elucidation of the Role of Msh4-Msh5 (MutSγ) in Homologous Recombination: A Biophysical and Biochemical Study. (Retrieved from 10.14418/wes01.3.99).

Lao JP, Cloud V, Huang CC, Grubb J, Thacker D, Lee CY, Dresser ME, Hunter N, and Bishop DK (2013a). Meiotic crossover control by concerted action of Rad51-Dmc1 in homolog template bias and robust homeostatic regulation. PLoS genetics 9, e1003978. [PubMed: 24367271]

Lao JP, Cloud V, Huang CC, Grubb J, Thacker D, Lee CY, Dresser ME, Hunter N, and Bishop DK (2013b). Meiotic Crossover Control by Concerted Action of Rad51-Dmc1 in Homolog Template Bias and Robust Homeostatic Regulation. PLoS Genetics 9.

Lao JP, Oh SD, Shinohara M, Shinohara A, and Hunter N (2008). Rad52 promotes postinvasion steps of meiotic double-strand-break repair. Molecular cell 29, 517–524. [PubMed: 18313389]

Leung WK, Humphryes N, Afshar N, Argunhan B, Terentyev Y, Tsubouchi T, and Tsubouchi H (2015). The synaptonemal complex is assembled by a polySUMOylation-driven feedback mechanism in yeast. The Journal of cell biology 211, 785–793.

Liebelt F, and Vertegaal AC (2016). Ubiquitin-dependent and independent roles of SUMO in proteostasis. Am J Physiol Cell Physiol 311, C284–296. [PubMed: 27335169]

Lin FM, Lai YJ, Shen HJ, Cheng YH, and Wang TF (2010). Yeast axial-element protein, Red1, binds SUMO chains to promote meiotic interhomologue recombination and chromosome synapsis. The EMBO journal 29, 586–596. [PubMed: 19959993]

Loidl J, and Lorenz A (2009). Analysis of Schizosaccharomyces pombe meiosis by nuclear spreading. Methods Mol Biol 558, 15–36. [PubMed: 19685316]

Macaisne N, Vignard J, and Mercier R (2011). SHOC1 and PTD form an XPF-ERCC1-like complex that is required for formation of class I crossovers. Journal of cell science 124, 2687–2691. [PubMed: 21771883]

Malkova A, Swanson J, German M, McCusker JH, Housworth EA, Stahl FW, and Haber JE (2004). Gene conversion and crossing over along the 405-kb left arm of Saccharomyces cerevisiae chromosome VII. Genetics 168, 49–63. [PubMed: 15454526]

Manhart CM, and Alani E (2016). Roles for mismatch repair family proteins in promoting meiotic crossing over. DNA repair 38, 84–93. [PubMed: 26686657]

Mazina OM, Mazin AV, Nakagawa T, Kolodner RD, and Kowalczykowski SC (2004). Saccharomyces cerevisiae Mer3 helicase stimulates 3'−5' heteroduplex extension by Rad51; implications for crossover control in meiotic recombination. Cell 117, 47–56. [PubMed: 15066281]

Mimitou EP, Yamada S, and Keeney S (2017). A global view of meiotic double-strand break end resection. Science 355, 40–45. [PubMed: 28059759]

Nakagawa T, and Kolodner RD (2002). Saccharomyces cerevisiae Mer3 is a DNA helicase involved in meiotic crossing over. Molecular and cellular biology 22, 3281–3291. [PubMed: 11971962]

Nayak A, and Muller S (2014). SUMO-specific proteases/isopeptidases: SENPs and beyond. Genome biology 15, 422. [PubMed: 25315341]

Oh SD, Lao JP, Hwang PY, Taylor AF, Smith GR, and Hunter N (2007). BLM ortholog, Sgs1, prevents aberrant crossing-over by suppressing formation of multichromatid joint molecules. Cell 130, 259–272. [PubMed: 17662941]

Owens S, Tang S, and Hunter N (2018). Monitoring Recombination During Meiosis in Budding Yeast. Methods Enzymol 601, 275–307. [PubMed: 29523236]

Papazian HP (1952). The analysis of tetrad data. Genetics 37, 175–188. [PubMed: 17247384]

Papouli E, Chen S, Davies AA, Huttner D, Krejci L, Sung P, and Ulrich HD (2005). Crosstalk between SUMO and ubiquitin on PCNA is mediated by recruitment of the helicase Srs2p. Molecular cell 19, 123–133. [PubMed: 15989970]

Perkins DD (1949). Biochemical Mutants in the Smut Fungus Ustilago Maydis. Genetics 34, 607–626. [PubMed: 17247336]

Qiao H, Prasada Rao HB, Yang Y, Fong JH, Cloutier JM, Deacon DC, Nagel KE, Swartz RK, Strong E, Holloway JK, et al. (2014). Antagonistic roles of ubiquitin ligase HEI10 and SUMO ligase RNF212 regulate meiotic recombination. Nature genetics 46, 194–199. [PubMed: 24390283]

Rao HB, Qiao H, Bhatt SK, Bailey LR, Tran HD, Bourne SL, Qiu W, Deshpande A, Sharma AN, Beebout CJ, et al. (2017). A SUMO-ubiquitin relay recruits proteasomes to chromosome axes to regulate meiotic recombination. Science 355, 403–407. [PubMed: 28059716]

Reynolds A, Qiao H, Yang Y, Chen JK, Jackson N, Biswas K, Holloway JK, Baudat F, de Massy B, Wang J, et al. (2013). RNF212 is a dosage-sensitive regulator of crossing-over during mammalian meiosis. Nature genetics 45, 269–278. [PubMed: 23396135]

Saito TT, and Colaiacovo MP (2017). Regulation of Crossover Frequency and Distribution during Meiotic Recombination. Cold Spring Harb Symp Quant Biol 82, 223–234. [PubMed: 29222342]

Schwacha A, and Kleckner N (1995). Identification of double Holliday junctions as intermediates in meiotic recombination. Cell 83, 783–791. [PubMed: 8521495]

Sekiyama N, Ikegami T, Yamane T, Ikeguchi M, Uchimura Y, Baba D, Ariyoshi M, Tochio H, Saitoh H, and Shirakawa M (2008). Structure of the small ubiquitin-like modifier (SUMO)-interacting motif of MBD1-containing chromatin-associated factor 1 bound to SUMO-3. The Journal of biological chemistry 283, 35966–35975. [PubMed: 18842587]

Serrentino ME, Chaplais E, Sommermeyer V, and Borde V (2013). Differential association of the conserved SUMO ligase Zip3 with meiotic double-strand break sites reveals regional variations in the outcome of meiotic recombination. PLoS genetics 9, e1003416. [PubMed: 23593021]

Sherman F (2002). Getting started with yeast. Methods Enzymol 350, 3–41. [PubMed: 12073320]

Snowden T, Acharya S, Butz C, Berardini M, and Fishel R (2004). hMSH4-hMSH5 recognizes Holliday Junctions and forms a meiosis-specific sliding clamp that embraces homologous chromosomes. Molecular cell 15, 437–451. [PubMed: 15304223]

Snowden T, Shim KS, Schmutte C, Acharya S, and Fishel R (2008). hMSH4-hMSH5 adenosine nucleotide processing and interactions with homologous recombination machinery. The Journal of biological chemistry 283, 145–154. [PubMed: 17977839]

Stahl FW (2008). On the “NPD ratio” as a test for crossover interference. Genetics 179, 701–704. [PubMed: 18493082]

Steinacher R, and Schar P (2005). Functionality of human thymine DNA glycosylase requires SUMO-regulated changes in protein conformation. Current biology : CB 15, 616–623. [PubMed: 15823533]

Sym M, and Roeder GS (1995). Zip1-induced changes in synaptonemal complex structure and polycomplex assembly. The Journal of cell biology 128, 455–466. [PubMed: 7860625]

Thacker D, Mohibullah N, Zhu X, and Keeney S (2014). Homologue engagement controls meiotic DNA break number and distribution. Nature 510, 241–246. [PubMed: 24717437]

Voelkel-Meiman K, Cheng SY, Parziale M, Morehouse SJ, Feil A, Davies OR, de Muyt A, Borde V, and MacQueen AJ (2019). Crossover recombination and synapsis are linked by adjacent regions within the N terminus of the Zip1 synaptonemal complex protein. PLoS genetics 15, e1008201. [PubMed: 31220082]

Voelkel-Meiman K, Taylor LF, Mukherjee P, Humphryes N, Tsubouchi H, and Macqueen AJ (2013). SUMO localizes to the central element of synaptonemal complex and is required for the full

synapsis of meiotic chromosomes in budding yeast. PLoS genetics 9, e1003837. [PubMed: 24098146]

Wach A, Brachat A, Pohlmann R, and Philippsen P (1994). New heterologous modules for classical or PCR-based gene disruptions in Saccharomyces cerevisiae. Yeast 10, 1793–1808. [PubMed: 7747518]

Wang S, Hassold T, Hunt P, White MA, Zickler D, Kleckner N, and Zhang L (2017). Inefficient crossover maturation underlies elevated aneuploidy in human female meiosis. Cell 168, 977–989 e917. [PubMed: 28262352]

Wang S, Liu Y, Shang Y, Zhai B, Yang X, Kleckner N, and Zhang L (2019). Crossover Interference, Crossover Maturation, and Human Aneuploidy. BioEssays : news and reviews in molecular, cellular and developmental biology 41, e1800221.

Watanabe Y (2012). Geometry and force behind kinetochore orientation: lessons from meiosis. Nature reviews. Molecular cell biology 13, 370–382. [PubMed: 22588367]

Wohlschlegel JA, Johnson ES, Reed SI, and Yates JR 3rd (2006). Improved identification of SUMO attachment sites using C-terminal SUMO mutants and tailored protease digestion strategies. J Proteome Res 5, 761–770. [PubMed: 16602682]

Xaver M, Huang L, Chen D, and Klein F (2013). Smc5/6-mms21 prevents and eliminates inappropriate recombination intermediates in meiosis. PLoS genetics 9, e1004067. [PubMed: 24385936]

Xu G, Paige JS, and Jaffrey SR (2010). Global analysis of lysine ubiquitination by ubiquitin remnant immunoaffinity profiling. Nat Biotechnol 28, 868–873. [PubMed: 20639865]

Yunus AA, and Lima CD (2009). Purification of SUMO conjugating enzymes and kinetic analysis of substrate conjugation. Methods Mol Biol 497, 167–186. [PubMed: 19107417]

Zakharyevich K, Ma Y, Tang S, Hwang PY, Boiteux S, and Hunter N (2010). Temporally and biochemically distinct activities of Exo1 during meiosis: double-strand break resection and resolution of double Holliday junctions. Molecular cell 40, 1001–1015. [PubMed: 21172664]

Zakharyevich K, Tang S, Ma Y, and Hunter N (2012). Delineation of joint molecule resolution pathways in meiosis identifies a crossover-specific resolvase. Cell 149, 334–347. [PubMed: 22500800]

Zhang L, Wang S, Yin S, Hong S, Kim KP, and Kleckner N (2014). Topoisomerase II mediates meiotic crossover interference. Nature 511, 551–556. [PubMed: 25043020]

Zhang Q, Ji SY, Busayavalasa K, and Yu C (2019). SPO16 binds SHOC1 to promote homologous recombination and crossing-over in meiotic prophase I. Sci Adv 5, eaau9780. [PubMed: 30746471]

Zhao X (2018). SUMO-Mediated Regulation of Nuclear Functions and Signaling Processes. Molecular cell 71, 409–418. [PubMed: 30075142]

Zickler D, and Kleckner N (2015). Recombination, pairing, and synapsis of homologs during meiosis. Cold Spring Harbor perspectives in biology 7, pii: a016626. doi: 016610.011101/cshperspect.a016626. [PubMed: 25986558]

Highlights

- Crossover factor Msh4 is a direct target of the SUMO E2-conjugase Ubc9
- Msh4 SUMOylation facilitates meiotic crossing over
- SUMOylation fosters interaction between Msh4 and Msh5
- Msh4 SUMOylation is triggered by DNA double-strand breaks

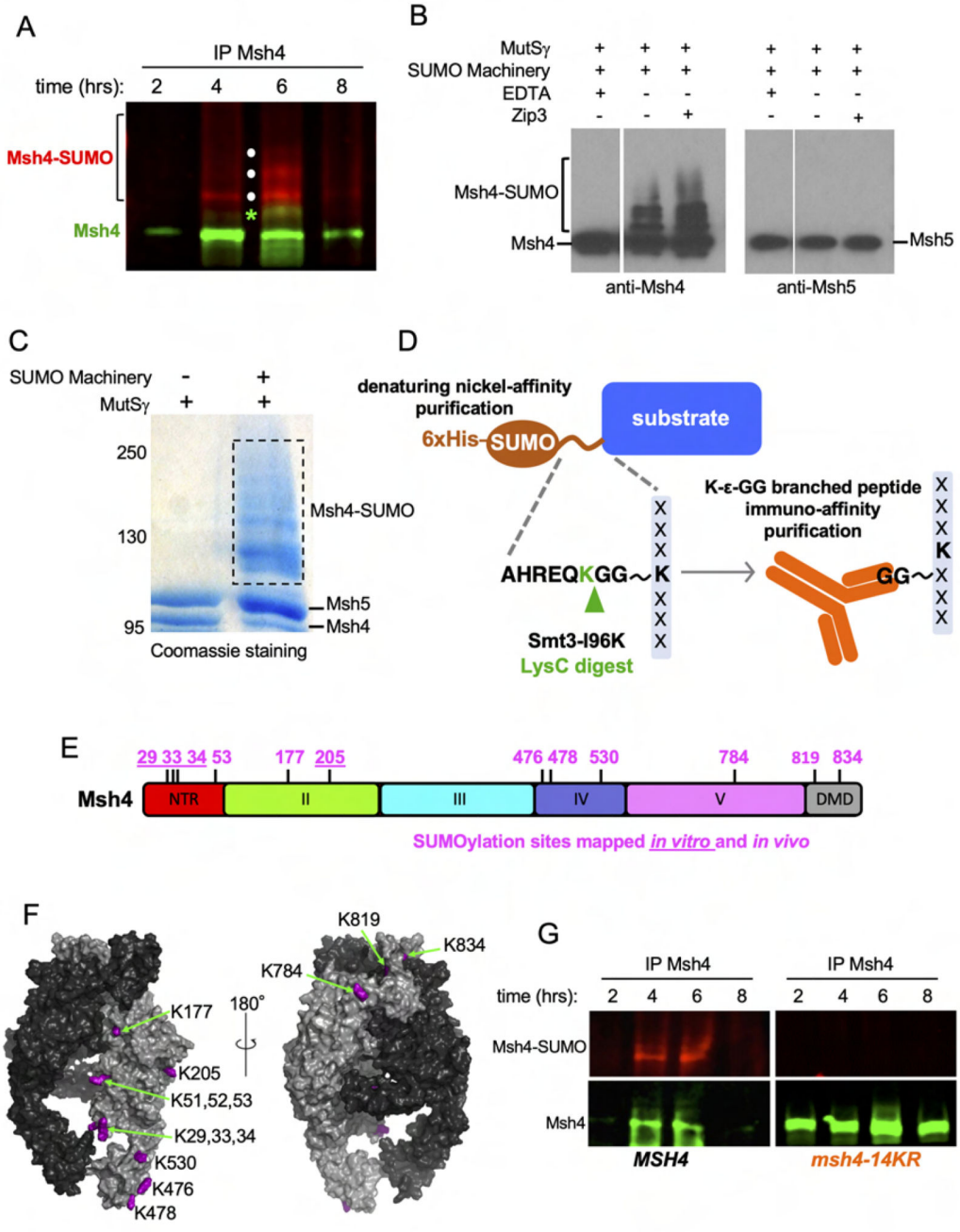

Figure 1. Msh4 SUMOylated and mapping of conjugation sites.

(A) IP-Western analysis of Msh4 SUMOylation throughout meiosis. Total Msh4 (green) and SUMOylated Msh4 (red) were simultaneously detected with anti-HA (detecting Msh4–3xHA) and anti-Smt3 antibodies, respectively, using the LI-COR Odyssey system. The green asterisk indicates the position of phosphorylated Msh4. White dots indicate the positions of SUMOylated forms of Msh4. (B) Western analysis of *in vitro* SUMOylation reactions containing purified MutSγ and with or without the E3 ligase Zip3. (C) Image of the SDS-PAGE gel used to isolate *in vitro* SUMOylated Msh4 for LC-MS/MS analysis. The

region excised for LC-MS/MS is indicated by a dashed box. (D) Schematic for global proteomics identification of SUMOylation sites using a tandem purification approach, first enriching for SUMO conjugates via nickel affinity purification of 6xHis tagged SUMO; and then immuno-purifying di-glycyl lysine branched remnants resulting from Lyc-C digestion (Bhagwat et al., 2021). (E) Positions of SUMOylated lysines on the Msh4 polypeptide mapped using the two complementary approaches described in C and D. SUMOylation sites identified from *in vitro* SUMOylated Msh4 (trypsin digestion) are underlined while sites identified by global proteomics (LysC ± GluC digests) are not. NTR, N-terminal region; DMD, dimerization domain. (F) 180° rotated views of a structure-based homology model of *S. cerevisiae* MutSγ, highlighting lysine residues identified as SUMOylation sites in magenta. In this space-filling model, the Msh4 subunit is shown in light grey and Msh5 is shown in black. (G) IP-Western analysis of Msh4 SUMOylation in wild-type *(MSH4)* and SUMOylation defective *(msh4–14KR)* strains. Twice the amount immunoprecipitated material was loaded for msh4–14KR samples to rule out the possibility that Msh4 was still being SUMOylated at a very low-level. Also see Supplemental Figures S1–S3.

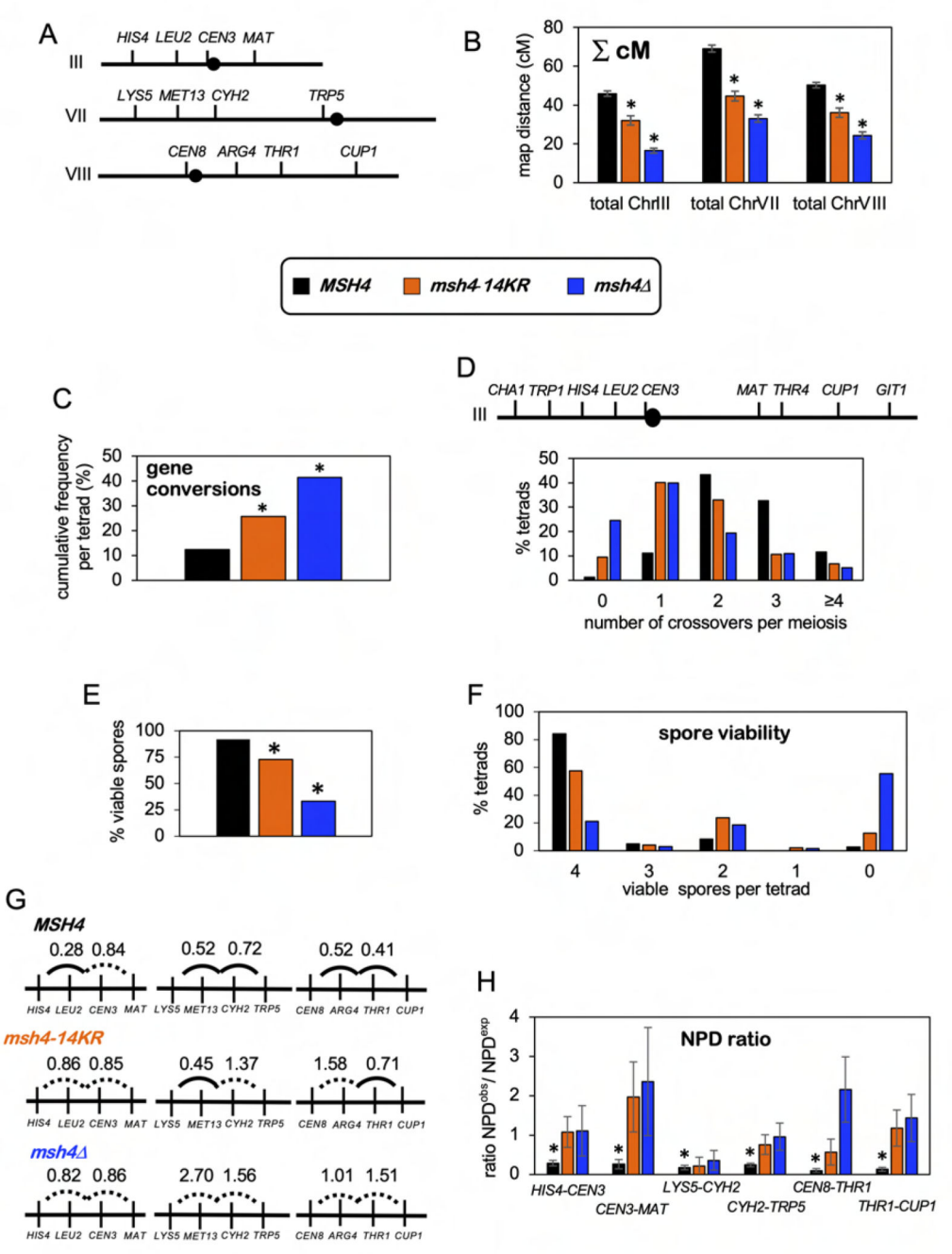

Figure 2. Msh4 SUMOylation facilitates crossing over, crossover assurance and crossover interference.

(A) Marker configurations in strains used to analyze recombination. *CEN3* and *CEN8* are heterozygously marked with the *ADE2* and *URA3* genes, respectively (Oh et al., 2007). (B) Cumulative map distances (± S.E.) for intervals on chromosomes III, VII and VIII. Asterisks indicate $p<0.05$ relative to wild type (*G*-test; see Table S2). (C) Cumulative frequencies of tetrads with gene conversions (non 2:2 segregations) for heterozygous alleles of the marker genes shown in (A). Asterisks indicate $p<0.01$ relative to wild type (z-test; (see Table S3). (D) Top: Marker configuration in strains used to analyze crossover assurance for

chromosome III. *CEN3* is heterozgously marked with the *LYS2 and URA3.* Bottom: Distributions of crossover classes for chromosome III (see Table S2). (E) Spore viabilities of indicated strains (see Table S4). (F). Distributions of tetrads with 4, 3, 2, 1 and 0 viable spores. (G). Interference analysis for adjacent intervals (Lao et al., 2013a; Malkova et al., 2004). Solid arcs between intervals indicate significant positive interference; failure to detect significant positive interference is indicated by dashed arcs (see Table S5). (H) Interference analysis within individual intervals expressed as NPD ratios (https://elizabethhousworth.com/StahlLabOnlineTools/). Error bars show S.E. Asterisks indicate significant positive interference (see Table S5). See also Figures S4 and S5.

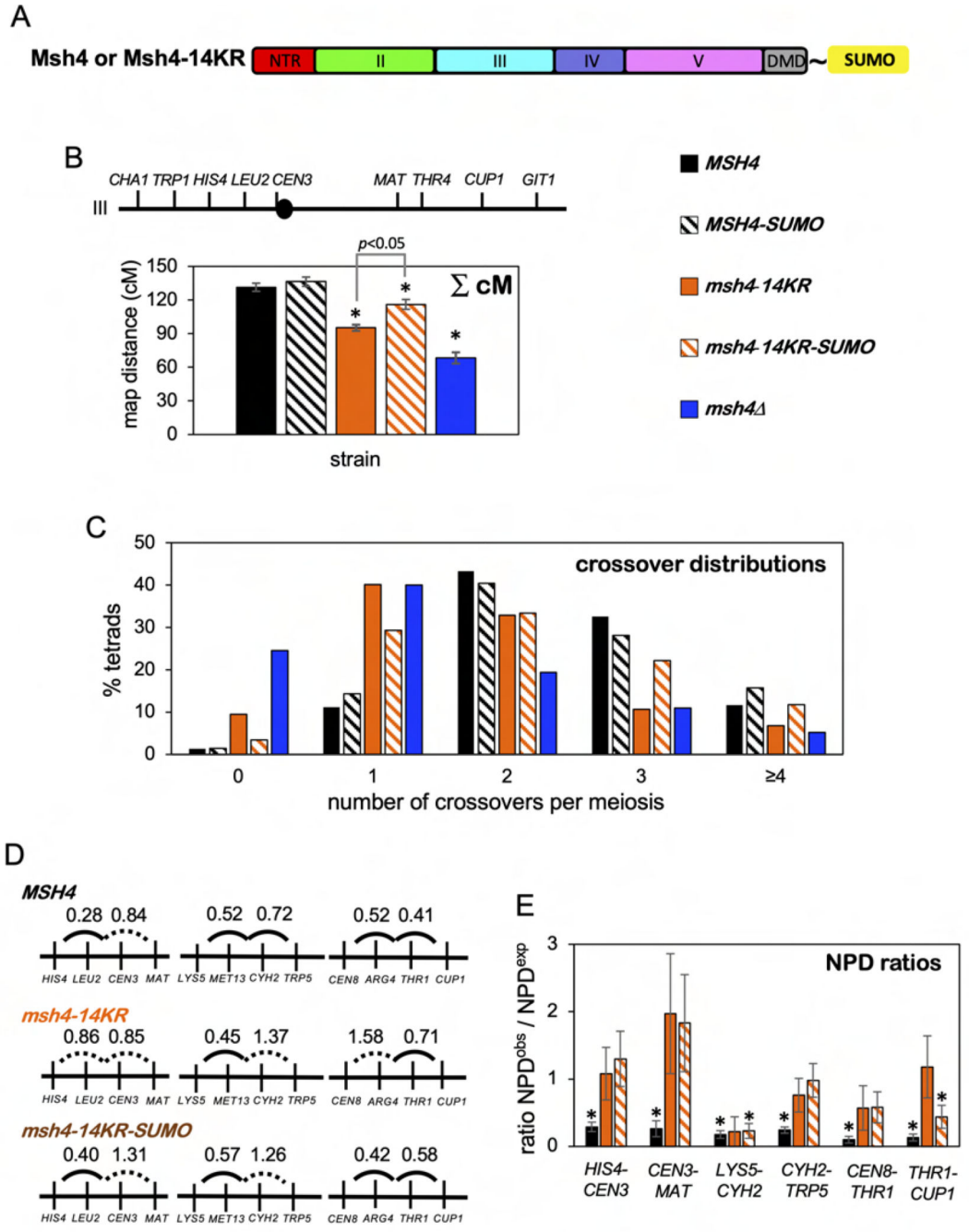

Figure 3. Fusion of SUMO to Msh4–14KR mitigates its crossover defect.

(A) Schematic illustrating the fusion of SUMO to the C terminus of Msh4 or msh4–14KR. "~" indicates a flexible linker (5'-GSGSGS-3') between Msh4 and SUMO. NTR, N-terminal region; DMD, dimerization domain. (B) Cumulative map distances (± S.E.) along chromosome III for the indicated genotypes. Asterisks indicate $p<0.05$ relative to wild type (*G*-test; see Table S2). (C) Distributions of crossover classes for chromosome III (see Table S2). See also Figure S6. (D) Interference analysis for adjacent intervals. Solid arcs between intervals indicate significant positive interference; failure to detect significant positive

interference is indicated by dashed arcs (see Table S5). (E) Interference analysis within individual intervals expressed as NPD ratios. Error bars show S.E. Asterisks indicate significant positive interference (see Table S5).

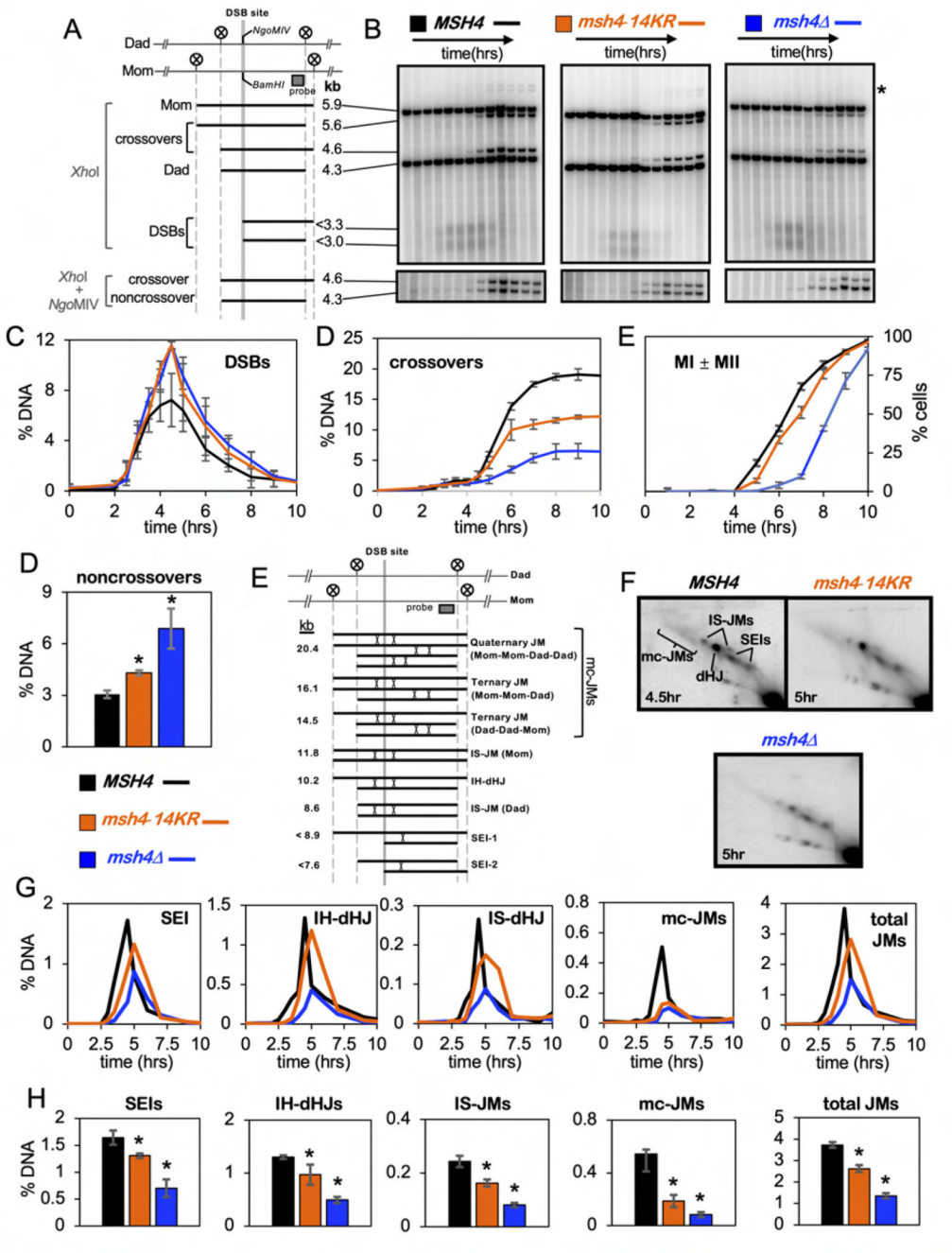

Figure 4. Msh4 SUMOylation facilitates joint-molecule processing.

(A) Map of the *HIS4:LEU2* locus highlighting the DSB site, *XhoI* restriction sites (circled Xs) and the position of the probe used in Southern blotting. Sizes of diagnostic fragments are shown below. (B) Representative 1D gel Southern blot images for analysis of DSBs, crossovers and noncrossovers. Time points are 0, 2, 2.5, 3, 3.5, 4, 4.5, 5, 6, 7, 9 and 11 hours. The asterisk highlights the position of bands corresponding to ectopic recombination between *HIS4::LEU2* and the native *LEU2* locus. (C) Quantification of DSBs, crossovers and meiotic divisions. %DNA is percentage of total hybridizing DNA signal. MI ± MII is

the percentage of cells that have completed one or both meiotic divisions. (D) Non-crossover levels at 11 hrs. Asterisks indicate $p<0.05$ relative to wild type (Student's *t*-test). (E) JM structures detected at the *HIS4:LEU2* locus. Positions of the DSB site, diagnostic *XhoI* sites (circled Xs) and the Southern probe are shown. (F) Representative 2D gel Southern blot images for time points where JM levels peak. Positions of the various JM signals are indicated in the first panel. (G) Quantification of JM species over time. (H) Quantification of JM species at their peak levels. IH-dHJs, inter-homolog dHJs; IS-JMs, intersister JMs (most likely dHJs); SEIs, single-end invasions; mcJMs, multi-chromatid JMs) and total JMs are quantified. Averages ± S.E. were calculated from three independent experiments.

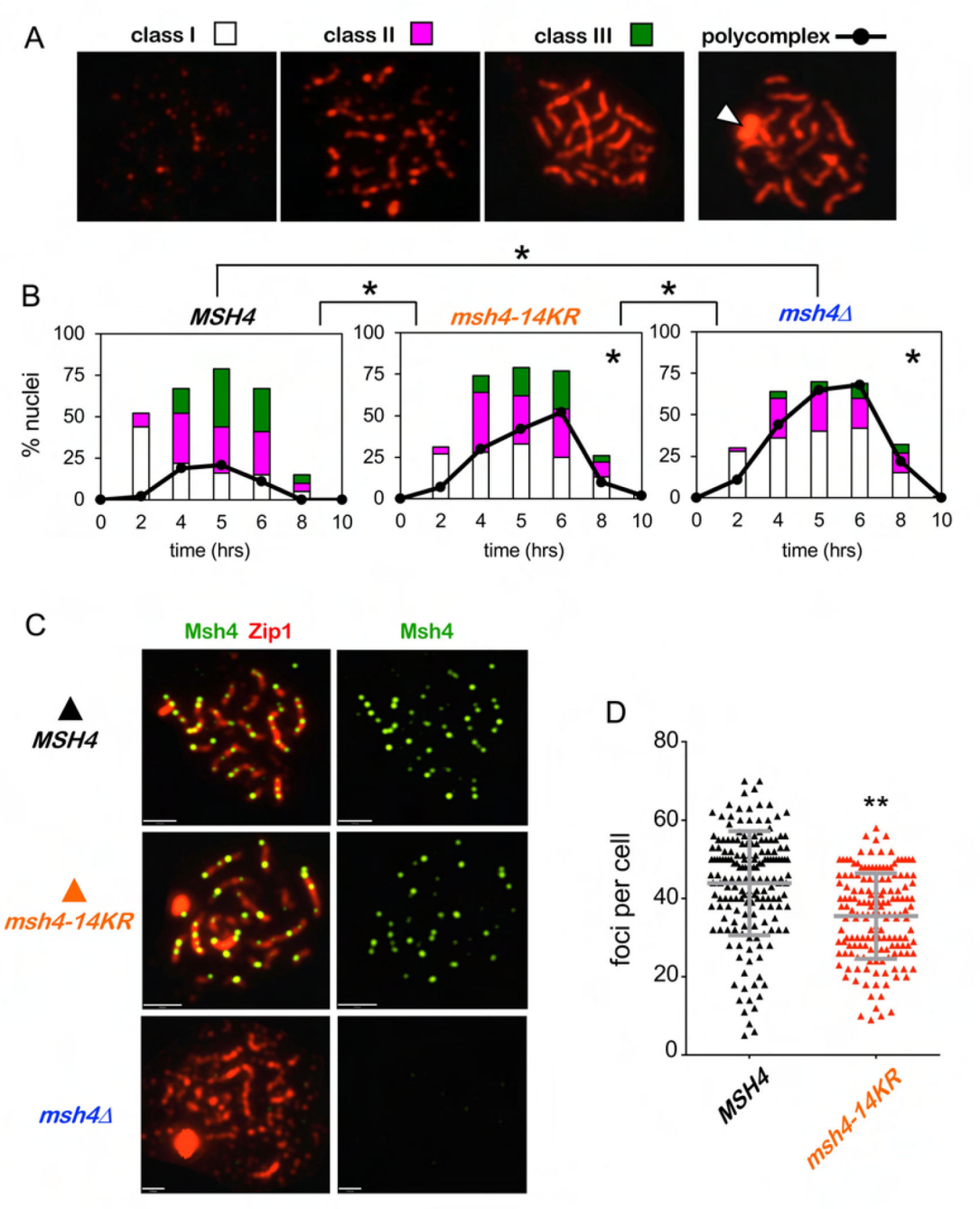

Figure 5. Msh4 SUMOylation facilitates homolog synapsis and enhances chromosomal localization of Msh4.

(A) Chromosome spreads showing representative examples of the three Zip1 immuno-staining classes and a nucleus containing a Zip1 polycomplex (highlighted by a caret). (B) Quantification of Zip1 staining classes and polycomplexes. ≥100 nuclei were scored for each time point. The color code is above the panels in A. *, $p<0.05$ two-tailed Mann-Whitney test. (C) Representative images of spread meiotic nuclei immuno-stained for Msh4 (green) and Zip1 (red). (D) Quantification of Msh4 immuno-staining foci in class II and class III

nuclei combined. ≥100 nuclei were scored for each strain. **, $p<0.005$ two-tailed Mann Whitney test. Scale bars = 30 μm. See also Figure S7.

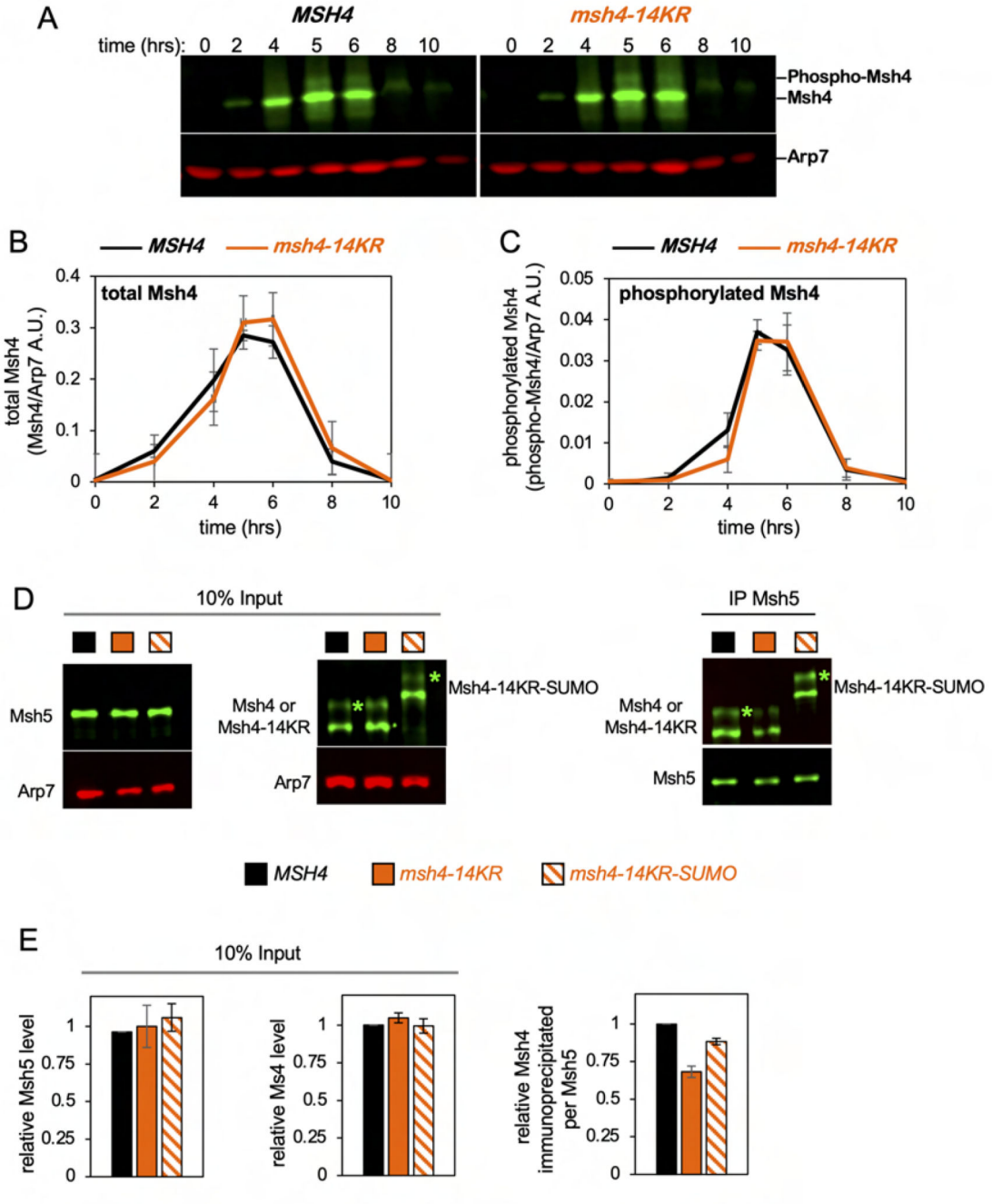

Figure 6. Msh4 SUMOylation enhances Msh4-Msh5 interaction.

(A) Representative Western analysis of Msh4 protein levels throughout meiosis in wild-type and *msh4–14KR* strains. (B) Quantification of total Msh4 and Msh4–14KR protein levels relative to the Arp7 loading control (Arbitrary Units, A.U.). Error bars represent means ± S.E from three independent experiments. (C) Quantification of levels of the slower-migrating phosphorylated isoform of Msh4, as in B. (D) Representative Western analysis of Msh4 and Msh5 protein levels in Msh5 immunoprecipitates from *MSH4, msh4–14KR* and *msh4–14KR-SUMO* strains. Left-hand side panels show analysis of 10% input cell extract;

Right-hand side panels show Msh5 immunoprecipitates. (E) Quantification of Western blots represented in D showing Msh4–14KR and Msh4–14KR-SUMO protein levels relative to those of wild-type Msh4 (right-hand side graphs); and levels of Msh4–14KR or Msh4–14KR-SUMO protein co-immunoprecipitated per Msh5 relative to wild type Msh4 (left-hand side graph). Error bars represent means ± S.E from three independent experiments.

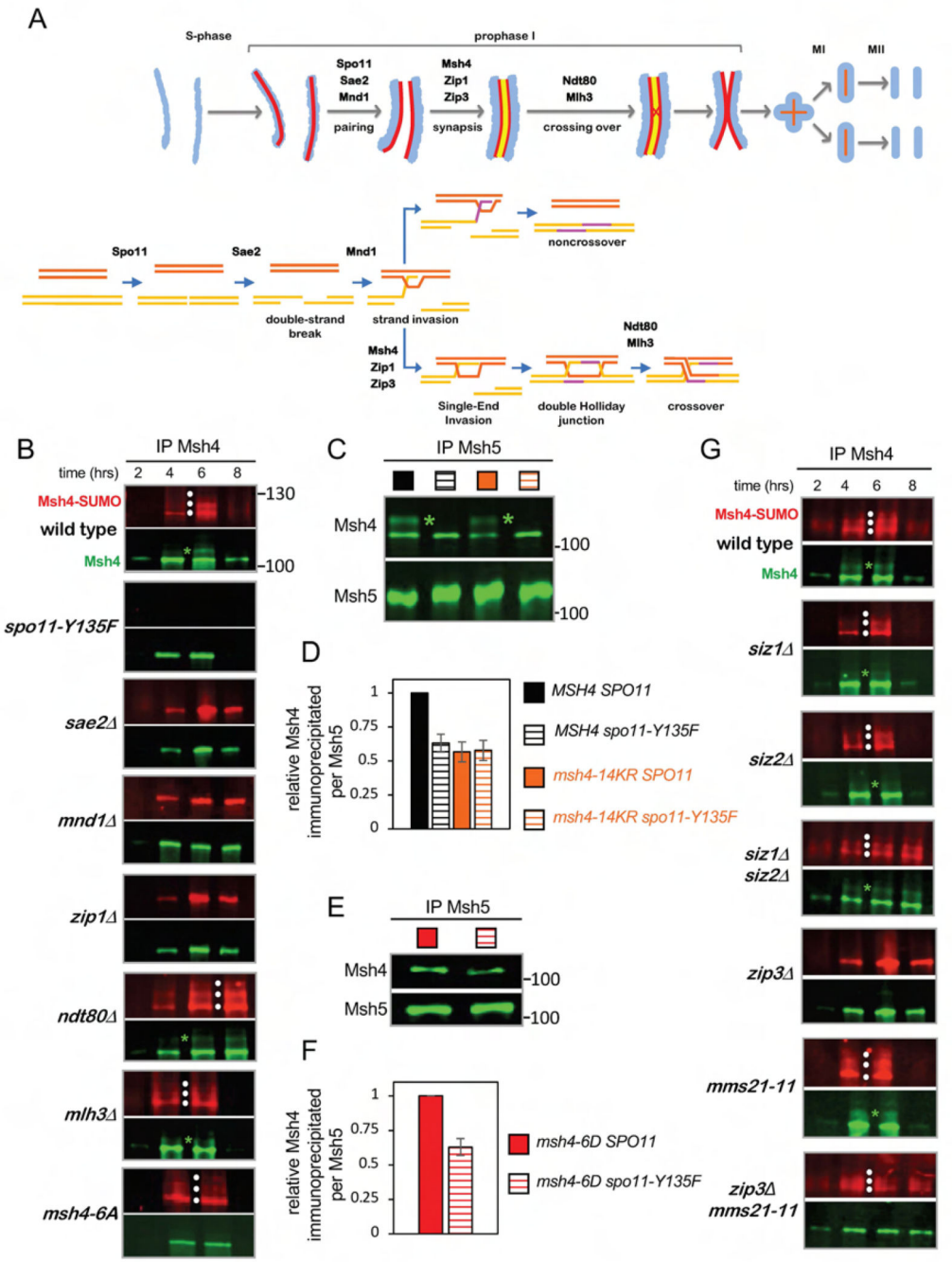

Figure 7. Genetic requirements for Msh4 SUMOylation.

(A) Chromosomal and recombination events of meiosis highlighting the steps affected by the mutants analyzed in panel B. Blue, chromatin; red lines, homolog axes; yellow line, synaptonemal complex central region. DNA events are shown for the two homologs involved in recombination. Magenta lines represent newly synthesized DNA. (B) Western analysis of total Msh4 (green) and SUMOylated Msh4 (red) in immunoprecipitates of Msh4 from strains with the indicated genotypes. Total and SUMOylated Msh4 were detected simultaneously using the LI-COR Odyssey system, but the individual channels are shown

for clarity (note that the wild-type panels are identical to those shown in Figure 1A). (C) Representative Western analysis of Msh4 and Msh5 protein levels in Msh5 immunoprecipitates from wild-type, *spo11-Y135F, msh4–14KR* and *msh4–14KR spo11-Y135F* strains. (D) Quantification of Western blots represented in C showing levels of Msh4 protein co-immunoprecipitated per Msh5 from wild-type, *spo11-Y135F, msh4–14KR* and *msh4–14KR spo11-Y135F* strains. Error bars represent means ± S.E from three independent experiments. (E) Representative Western analysis of Msh4 and Msh5 protein levels in Msh5 immunoprecipitates from *msh4–6D* and *msh4–6D spo11-Y135F* strains. (F) Quantification of Western blots represented in E showing levels of Msh4 co-immunoprecipitated per Msh5 from *msh4–6D* and *msh4–6D spo11-Y135F* strains. Error bars represent means ± S.E from three independent experiments. (G) Western analysis of Msh4 SUMOylation in the indicated mutants of the SUMO E3 ligases Siz1, Siz2, Zip3 and Mms21. The green asterisks indicate the position of phosphorylated Msh4. White dots indicate the positions of SUMOylated forms of Msh4. See also Figure S8.

KEY RESOURCES TABLE

REAGENT or RESOURCE	SOURCE	IDENTIFIER
Antibodies		
Mouse Anti-HA Monoclonal antibody, Unconjugated, Clone 12CA5	Millipore Sigma	Cat# 11583816001, RRID:AB_514505
Mouse Anti-FLAG M2 Mouse Monoclonal antibody	Millipore Sigma	Ca#: F3165 RRID: AB_259529
Smt3 rabbit polyclonal antibody	Gift from Dr. Steve Brill, Rutgers University.	N/A
Arp7 (yN-20) antibody	Santa Cruz Biotechnology	Cat# sc-8960, RRID:AB_671731
IRDye® 800CW Donkey anti-Mouse IgG antibody	LI-COR Biosciences	Cat#:925-32212
IRDye® 680LT Donkey anti-Goat IgG antibody	LI-COR Biosciences	Cat#: 925-68024
IRDye® 680LT Donkey anti-Rabbit IgG antibody	LI-COR Biosciences	Cat#: 925-68023
IRDye® 800CW Donkey anti-Rabbit IgG antibody	LI-COR Biosciences	Cat#: 925-32213
Msh4 polyclonal antibody	Gift from Dr. A. Shinohara, Osaka University	N/A
Msh5 polyclonal antibody		N/A
Zip1 polyclonal antibody		N/A
Chemicals, Peptides, and Recombinant Proteins		
Msh4-Strep–Msh5-His	This paper	N/A
Critical Commercial Assays		
QuikChange Lightning Site-Directed Mutagenesis Kit	Agilent Technologies	Ca#: 210518
Prime-It RmT Random Primer Labeling Kit	Stratagene	Ca#: 300392
Gibson Assembly® Cloning Kit	New England Biolabs	Ca#: E5510S
Experimental Models: Organisms/Strains		
Saccharomyces cerevisiae; for individual genotypes see Table S7	N/A	N/A
Oligonucleotides		
See Table S6 for primers used in this study		
Recombinant DNA		
pUC18-Msh4-3HA-KanMX4 (pNH 600)	This paper	N/A
pFA6a-natMX4-pGAL1 -3HA	Gift of Dr. A. Amon, MIT (Chan and Amon, 2010)	N/A
pFA6a-3HA-kanMX4		(Wach et al., 1994)
pFA6a-3HA-hphMX4		(Wach et al., 1994)
pFA6a-GFP-kanMX4		(Wach et al., 1994)
pET15b-Aos1	Gift of Dr. C. Lima, Sloan-Kettering Institute (Yunus and Lima, 2009)	N/A
pET28b-Uba2		
pET28b-Ubc9		
pET28b-Smt3		
Software and Algorithms		

REAGENT or RESOURCE	SOURCE	IDENTIFIER
Volocity 6.3	Perkin Elmer	N/A
Image Studio Lite 4.0	LI-COR Biosciences	N/A
Scaffold 4.8.1	Proteome Software	N/A
Stahl Lab online tool	http://elizabethhousworth.com/StahlLabOnlineTools/	
Vassarstats online tool	http://vassarstats.net/newcs.html	